haematologica
Journal of The Ferrata Storti Foundation

# Comprehensive genomic analysis of refractory multiple myeloma reveals a complex mutational landscape associated with drug resistance and novel therapeutic vulnerabilities

by Nicola Giesen, Nagarajan Paramasivam, Umut H. Toprak, Daniel Huebschmann, Jing Xu, Sebastian Uhrig, Mehmet Samur, Stella Bähr, Martina Fröhlich, Sadaf S. Mughal, Elias K. Mai, Anna Jauch, Carsten Müller-Tidow, Benedikt Brors, Nikhil Munshi, Hartmut Goldschmidt, Niels Weinhold, Matthias Schlesner, and Marc S. Raab

*Received: June 7, 2021.*
*Accepted: January 7, 2022.*

*Citation: Nicola Giesen, Nagarajan Paramasivam, Umut H. Toprak, Daniel Huebschmann, Jing Xu, Sebastian Uhrig, Mehmet Samur, Stella Bähr, Martina Fröhlich, Sadaf S. Mughal, Elias K. Mai, Anna Jauch, Carsten Müller-Tidow, Benedikt Brors, Nikhil Munshi, Hartmut Goldschmidt, Niels Weinhold, Matthias Schlesner, and Marc S. Raab. Comprehensive genomic analysis of refractory multiple myeloma reveals a complex mutational landscape associated with drug resistance and novel therapeutic vulnerabilities.*
*Haematologica. 2022 Jan 20. doi: 10.3324/haematol.2021.279360. [Epub ahead of print]*

# Comprehensive genomic analysis of refractory multiple myeloma reveals a complex mutational landscape associated with drug resistance and novel therapeutic vulnerabilities

Running head: Genomic analysis of refractory multiple myeloma

Nicola Giesen[1,2]*, Nagarajan Paramasivam[3,4]*, Umut H Toprak[3,5]*, Daniel Huebschmann[4,6,7,8]*, Jing Xu[1,2,9], Sebastian Uhrig[4,9], Mehmet Samur[10,11], Stella Bähr[4], Martina Fröhlich[4,9], Sadaf S Mughal[9], Elias K Mai[1], Anna Jauch[12], Carsten Müller-Tidow[1,13], Benedikt Brors[8,9,13], Nikhil Munshi[14], Hartmut Goldschmidt[1,13], Niels Weinhold[1#], Matthias Schlesner[3#], Marc S Raab[1,2#]

[1]Department of Internal Medicine V, Heidelberg University Hospital, Heidelberg, Germany

[2]Clinical Cooperation Unit Molecular Hematology/Oncology, Department of Internal Medicine V, Heidelberg University Hospital, and German Cancer Research Center (DKFZ), Heidelberg, Germany

[3]Bioinformatics and Omics Data Analytics, German Cancer Research Center (DKFZ), Heidelberg, Germany

[4]Computational Oncology, Molecular Diagnostics Program, National Center for Tumor Diseases (NCT) Heidelberg and German Cancer Research Center (DKFZ) Heidelberg, Germany

[5]Division of Neuroblastoma Genomics, German Cancer Research Center (DKFZ), Heidelberg, Germany

[6]Heidelberg Institute for Stem cell Technology and Experimental Medicine (HI-STEM), Heidelberg, Germany

[7]Department of Pediatric Immunology, Hematology and Oncology, Heidelberg University Hospital, Heidelberg, Germany

[8]German Cancer Consortium (DKTK), Core Center Heidelberg, Germany

[9]Division of Applied Bioinformatics, German Cancer Research Center (DKFZ), Heidelberg, Germany

[10]Department of Data Sciences, Dana-Farber Cancer Institute, Boston, MA, USA

[11]Department of Biostatistics, Harvard TH Chan School of Public Health, Boston, MA, USA

[12]Institute for Human Genetics, Heidelberg University Hospital, Heidelberg, Germany

[13]National Center for Tumor Diseases (NCT), Heidelberg, Germany

[14]Jerome Lipper Multiple Myeloma Center, Department of Medical Oncology, Dana-Farber Cancer Institute, Boston, MA, USA.

*NG, NP, UHT, and DH co-first authors

[#]NW, MS, and MSR co-senior authors

Corresponding author:

Marc S. Raab, Heidelberg Myeloma Center, Department of Internal Medicine V, Heidelberg University Hospital, Im Neuenheimer Feld 410, 69120 Heidelberg, Germany, phone: +49-6221-567031, fax: +49-6221-566163, email: m.raab@dkfz-heidelberg.de and nicola.giesen@med.uni-heidelberg.de

Data availability:

Sequence data has been made available at the European Genome-phenome Archive (EGAS00001004363).

Word count:

Abstract: 211

Main text: 3454

Number of tables: 0

Number of figures: 5

Number of supplementary files: 3

## Authors' contributions:

N.G., N.W., M.S., and M.S.R. designed the study, collected and analyzed data, and wrote the paper. N.P., U.H.T., and D.H. analyzed data and wrote the paper. J.X., S.U., S.B., M.F., S.S.M., A.J., and B.B. analyzed data. E.K.M., C.M.T., N.M., and H.G. collected data. All authors critically reviewed and approved the final version of the manuscript.


## Acknowledgments:

The authors would like to thank Anja Baumann, Katrin Pfütze and Bettina Meißburger, the DKFZ Omics IT and Data Management Core Facility, and the DKFZ Genomics and Proteomics Core Facility for excellent technical support, the Heidelberg Center for Personalized Oncology (DKFZ-HIPO), the Dietmar-Hopp Foundation, the Olympia-Morata program, Novartis and Amgen for funding support. BB received funding from the ERC under the European Union's Horizon 2020 research and innovation program (grant agreement n°825835), MS and NM received funding from NIH (grants P50-CA100707 and P01-CA155258). We especially thank all the patients and their families for their participation in this study.

## Abstract

The outcomes of patients with multiple myeloma (MM) refractory to immunomodulatory agents (IMiDs) and proteasome inhibitors (PIs) remain poor. We performed whole genome and transcriptome sequencing of 39 heavily pretreated relapsed/refractory MM (RRMM) patients to identify mechanisms of resistance and potential therapeutic targets. We observed a high mutational load and indications of increased genomic instability. Recurrently mutated genes in RRMM, which had not been previously reported or only observed at a lower frequency in newly diagnosed MM, included *NRAS*, *BRAF*, *TP53*, *SLC4A7*, *MLLT4*, *EWSR1*, *HCFC2*, and *COPS3*. We found multiple genomic regions with bi-allelic events affecting tumor suppressor genes and demonstrated a significant adverse impact of bi-allelic *TP53* alterations on survival. With regard to potentially resistance conferring mutations, recurrently mutated gene networks included genes with relevance for PI and IMiD activity, the latter particularly affecting members of the Cereblon and the COP9 signalosome complex. We observed a major impact of signatures associated with exposure to melphalan or impaired DNA double-strand break homologous recombination repair in RRMM. The latter coincided with mutations in genes associated with PARP inhibitor sensitivity in 49% of RRMM patients, a finding with potential therapeutic implications. In conclusion, this comprehensive genomic characterization revealed a complex mutational and structural landscape in RRMM and highlights potential implications for therapeutic strategies.

## Introduction

The introduction of novel therapies such as immunomodulatory agents (IMiDs) and proteasome inhibitors (PIs) has improved the outcomes of patients with multiple myeloma (MM) including those with relapsed MM (RMM) following second or third lines of therapy.[1] However, survival remains short if the disease becomes resistant to the major drug classes despite the advent of monoclonal antibodies.[2, 3] Relapsed/refractory MM (RRMM) therefore represents a patient population of particularly high unmet medical need.[4] Thus, a better understanding of the pathophysiology of RRMM is key to improving outcome of these patients.

In recent years, advances have been made in elucidating the genomic landscape of newly diagnosed MM (NDMM). These studies have revealed marked clonal heterogeneity with recurrently mutated genes each only affecting a minority of patients.[5-7] Clonal evolution over the course of the disease caused both by therapeutic interventions and ongoing genetic instability leads to more resistant clones in RMM, and finally to RRMM.[8-11] Accordingly, RRMM represents, in many respects, a fundamentally different biological disease entity. However, in contrast to NDMM, genomic data on RRMM is still limited.

Data from targeted sequencing in RRMM has identified an evolved set of mutated genes with enrichment for certain oncogenic drivers such as *KRAS*, *NRAS*, and *TP53* mutations and the development of what are presumed to be resistance-associated mutations.[11] Mutations conferring resistance to PIs and IMiDs have been described in proteasomal subunits and in the IMiD target gene *Cereblon* (*CRBN*), respectively.[11, 12] It is noteworthy that most of these mutations only occur in a minority of patients and at low allele frequency.[13] Additional mechanisms of resistance may therefore be important in RRMM. An unbiased and comprehensive molecular study is therefore required to fully dissect the biology underlying RRMM.

Here, we used whole genome sequencing (WGS) and RNA sequencing (RNA-Seq) to comprehensively analyze a highly selected cohort of 39 heavily pretreated RRMM patients with at least double

refractory disease, revealing a complex mutational and structural landscape and highlighting potential implications for personalized therapeutic strategies.

## Methods

### Patient characteristics

WGS and RNA-Seq was performed on samples from 39 highly refractory MM patients. Nine of these samples have been analyzed and reported before by our group using targeted sequencing.[11] The median number of prior therapy lines was 5 (2-13), all had relapsed following IMiDs and PIs, and 34 (87%) had had an autologous transplant. All patients were at least double-refractory, 62% were at least triple-refractory, and 38% were quadruple-refractory to IMiDs and PIs (**suppl Table S1**). In addition, 8% were also refractory to anti-CD38 monoclonal antibodies. Median progression-free survival (PFS) calculated from the time of sampling was 3.5 months and median overall survival (OS) was 7.4 months. Using fluorescence in situ hybridization (FISH)-based methods, 21 (54%) RRMM patients harbored high-risk cytogenetic aberrations. Specifically, 16 (41%) had deletion 17p. For comparison with NDMM, we further analyzed a WGS data set of 21 NDMM patients. For comparative analyses of mutational signatures, we included WGS data of 15 RMM patients with a median of two (1-4) prior therapy lines, thus less heavily pretreated than our RRMM cohort. Both additional WGS data sets are publicly available and had a median coverage of 40x.[14, 15]

### Sample acquisition and preparation

Between March 2014 and October 2017, tumor samples from 39 RRMM patients were collected at Heidelberg University Hospital. Written informed consent was obtained prior to sampling in accordance with the Declaration of Helsinki. This study was approved by the Institutional Ethics Committee.

CD138+ plasma cells were isolated as described previously.[11] DNA and RNA were extracted using the AllPrep kit (QIAGEN, Hilden, Germany). Saliva, buccal swabs or bone marrow stroma cells obtained from cultured CD138- cells were used as germline controls. Saliva was collected in Oragene-Dx tubes

and DNA was extracted using prepIT-L2P (DNA Genotek, Ottawa, Canada). DNA from buccal swabs was extracted using the blackPREP Swab DNA Kit (Analytik Jena, Jena, Germany). DNA from stroma cells was extracted using the QIAamp DNA Mini Kit (QIAGEN, Hilden, Germany).

## Whole genome sequencing

As described previously,[16] DNA libraries were prepared following the Illumina TruSeq Nano DNA Library protocol using the TruSeq DNA Nano kit (Illumina, Hayward, CA) and then sequenced on two lanes on the HiSeq X (2×151 bp) using the HiSeq X Ten Reagent Kit v2.5 (Illumina, Hayward, CA) to a median coverage of 77x.

## Alignment and small variant calling

The raw reads were mapped to the human reference genome (build 37, version hs37d5), using BWA mem[17] (version 0.7.8). To assess the effect of differing sequencing depths between the NDMM (median coverage 40x), RMM (40x), and RRMM (77x) samples on variant calling, subsampling of RRMM samples was performed for comparative analyses using Sambamba[18] (version 0.6.6) to achieve a 50% lower coverage.

Small nucleotide variants (SNVs) were called using SAMtools mpileup (version 0.1.19) and bcftools view. Indels were called using Platypus[19] (version 0.8.1). Variants were annotated with Gencode[20] (version 19) and ANNOVAR[21]. Splicing SNVs or SNVs resulting in nonsynonymous coding were called 'functional SNVs'. For prediction of functional relevance of SNVs, we calculated Combined Annotation Dependent Depletion (CADD) scores (version 1.3) and used a cut-off of 20. Driver genes were identified using IntOGen[22] (version 3.0.5).

## Analysis of mutational signatures and Kataegis clusters

A supervised analysis of mutational signatures was performed with the R package YAPSA,[23] based on the mutational catalogue of the 30 known signatures from COSMIC v2 (https://cancer.sanger.ac.uk/signatures/signatures_v2), supplemented with the MM1 signature which was recently linked to melphalan exposure.[15, 24] We defined Kataegis-like clusters to be regions

of increased SNV density with at least five SNVs with at most 1000 bp inter-mutational distance in one sample.[25]

## Calculation of HRDetect scores

HRDetect is a weighted model used to predict BRCA1/2 deficient tumors.[26] We used an implementation of HRDetect available at https://github.com/eyzhao/hrdetect-pipeline.[27]

## Detection of copy number variation and structural variants

Copy number states were called as described previously,[16, 25] and estimation of tumor purity and ploidy was performed using ACEseq (allele-specific copy number estimation from sequencing; https://www.biorxiv.org/content/early/2017/10/29/210807).

Structural variants (SVs) were detected using the DKFZ SOPHIA workflow (version 2.0.2, https://github.com/DKFZ-ODCF/SophiaWorkflow).[16, 25] SV candidate detection is a process of split-read and discordant mate evidence collection across each breakpoint as precursors for a SV. SV candidates (pairs of breakpoints) are filtered by a complex decision tree trained by expert assessment of orthogonal FISH data.

## RNA sequencing

RNA-Seq libraries were prepared using the Illumina TruSeq stranded mRNA kit and were sequenced on the Illumina HiSeq 2000 V4 platform. The paired-end reads were mapped to the STAR index generated reference genome (build 37, version hs37d5) with gencode (version 19) using STAR[28] (version 2.5.2b). The gene expressions were quantified using featureCounts (Subread version 1.5.1). Gene fusions were detected using Arriba version 1.0.0 (https://github.com/suhrig/arriba) as described previously.[29]

A detailed description of the bioinformatics workflow and subsequent analyses is provided in supplemental methods.

## Results

### High mutational load and genomic instability in RRMM

RRMM displayed a complex mutational landscape and an increase of both chromosomal and nucleotide aberrations compared to NDMM (**Figure 1A**, **suppl. Figure S1**). With a median of 67 (range 7-496), the overall load of SVs was significantly higher in RRMM (p=0.002) (**Figure 1B**, **suppl. Figure S1**). Complex structural rearrangements and catastrophic events were a frequent finding in RRMM patients, notably chromoplexy (n=10) and chromothripsis (n=5) (**Figure 1C, D**). Numerical chromosomal aberrations, which occurred significantly more frequently in RRMM compared to NDMM, included gain(1q) and deletions of 1p, 13q, and 17p (all p<0.05, **suppl. Figure S1**).

The overall mutational load in RRMM was also significantly higher than in NDMM ($p<10^{-5}$) (**Figure 1E**, **suppl. Figure S1**). We observed a median number of 116 (range 42-237) functional SNVs and 5 (range 1-15) functional indels per patient and overall, a median of 3.94 somatic small variants per megabase in RRMM. RRMM patients showed a much higher prevalence of SNVs outside of Kataegis-like clusters than NDMM patients ($p<10^{-5}$) indicating activity of mutational mechanisms on a broader scale in RRMM (**suppl. Figure S1**).

Genomic instability, assessed by calculation of the unbiased sum of homologous recombination deficiency (HRD), large-scale transition (LST) and telomeric allelic imbalance (TAI) scores, was significantly increased in RRMM compared to NDMM (p=0.004, **Figure 1F**, **suppl. Figure S1**).

### Driver gene aberrations in RRMM

Significantly mutated driver genes in RRMM featured prominently members of the mitogen-activated kinase pathway and *TP53* (**Figure 2, suppl. Table S2**) and showed large overlap to known drivers in NDMM. However, the prevalence of *BRAF* (p<0.001) and *TP53* (p<0.0001) mutations was significantly higher in RRMM compared to data from NDMM patients published by Walker *et al*;[7] a trend was also seen for *NRAS* mutations (p=0.05). In addition, we identified the following genes as significantly mutated drivers in RRMM: the sodium bicarbonate co-transporter SLC4A7 (13%), the Ras target

MLLT4 (5%), the RNA binding protein EWSR1 (5%), the MLL complex member HCFC2 (5%), and the COP9 signalosome subunit COPS3 (5%) (**Figure 2**). RNA Seq data confirmed expression of the vast majority of variants. Virtually all variants were predicted to be functionally relevant by CADD score (**suppl. Figure S2**).

We found multiple bi-allelic events or 'double hits' in RRMM affecting known tumor suppressor genes (TSGs) (**suppl. Table S3**). In total, 25 of 39 RRMM patients presented with at least one double hit in TSGs, significantly increased compared to NDMM (3/21, p<0.001). The most frequently affected TSGs in RRMM were *TP53* (n=8), *RB1* (n=7), and *TRAF3* (n=6). RRMM patients with a double hit of *TP53* had significantly inferior PFS (p=0.004) and a trend for inferior OS (p=0.07), both calculated from time of sampling, in univariate log-rank tests compared to patients with no or a single hit of *TP53* (**Figure 3**). While treatment of patients before and after sampling was heterogeneous, the adverse impact of bi-allelic TP53 alterations remained significant in multivariate analysis including age, number of prior therapies and ISS as possible confounders with regard to both PFS (hazard ratio (HR) 4.02; p=0.01) and OS (HR 4.77; p=0.02). 'Double hits' in other single TSGs or a combination thereof did not show a significant impact on survival which would have been independent of TP53 events.

## Oncogenic networks in RRMM

Next, we analyzed whether gene groups, resistance mechanisms or signaling networks were recurrently affected by small variants in our RRMM cohort (**suppl. Table S4**). We first addressed genes linked to the mechanisms of action of PIs and IMiDs (**suppl. Figure S3-5, suppl. Table S5**). Overall, 21% of RRMM patients as opposed to only 5% of NDMM patients harbored mutations in genes considered relevant to PI activity, mainly proteasome subunits (PSMB5, PSMC2, PSMC6, PSMD2, PSMD11, and PSME3). Recurrent mutations were also detected in TJP1, previously found to modulate PI sensitivity in MM.[30] However, statistical significance was not reached (p=0.14), likely due to the limited sample size. Regarding IMiD resistance, candidate mutations were found to be significantly more frequent in RRMM patients compared to NDMM (31% vs. 5%, p=0.02). We

observed mutations in all four members of the CRBN complex (*CRBN*, *CUL4B*, *RBX1*, *DDB1*), *IZKF1* as downstream target, as well as in three members of the COP9 signalosome complex (*COPS3*, *COPS4*, *COPS8*) and *CAND1*, which are regulators of cullin-RING ligase neddylation and which were recently identified in a CRISPR-Cas9 screen as essential for IMiD mechanism of action.[31]

The MAPK pathway harbored mutations in 77% of RRMM patients (52% in NDMM), mostly due to mutations in *NRAS*, *KRAS* and *BRAF*. NFKB signaling was affected in 23% (5% in NDMM) with recurrent mutations in *NFKB1*, *NFKB2*, *TRAF3* and *CHUK*. Both pathways showed a trend to being more frequently affected in RRMM, as did the large functional group of epigenetic modifiers which was affected in 77% of RRMM patients (52% in NDMM, all p=0.08). Of potential therapeutic interest, mutations in genes associated with sensitivity to PARP inhibitors were found in 49% of RRMM compared to 29% of NDMM patients, however, not reaching statistical significance (p=0.17), with recurrent mutations in *ATM*, *NBN*, and *TOP3A* (**suppl. Figure S3, S6, suppl. Table S5**).

## Enrichment of mutational signatures of impaired DNA damage repair in RRMM

To identify mechanisms contributing to high mutational load and high genomic instability observed in RRMM as compared to NDMM, we analyzed mutational signatures (**Figure 4A**, **suppl. Figure S7**). For further evaluation of different disease stages, we also included a cohort of relapsed but less heavily pretreated RMM patients as an intermediate stage, which had previously been analyzed by Maura et al.[15] In supervised fitting with signature-specific cutoffs, we found a significantly higher contribution from COSMIC signatures AC3 (associated with deficiency in homologous recombination repair) and the melphalan signature MM1 (p=0.006 and p<0.001, resp.) in RRMM compared to NDMM (**Figure 4B**) at the cost of the clock-like signatures AC1 (spontaneous deamination) and AC5 (clock-like but unknown) with significantly lower contributions (p<0.001 and p=0.005, resp.). In RMM, we detected signature MM1, but to a lesser extent when compared to our RRMM cohort (p=0.004), and signature AC3 was found with exposures in-between the NDMM and RRMM cohorts (**Figure 4A**, **suppl. Figure S7**). Comparison of the clinical information on the published RMM cohort with our RRMM patients confirmed a significantly higher overall number of prior therapies as well as more extensive exposure

to both novel agents and to high-dose melphalan therapy in our RRMM patients. Information on all mutational signatures detected in this manuscript including asserted mutational mechanisms is summarized in **suppl. Table S6**.

To further assess the finding of enriched deficiency in homologous recombination repair as indicated by signature AC3, we applied HRDetect, which is a weighted model used to predict BRCA1/2 deficient tumors.[26] HRDetect scores were significantly higher in RRMM than in both NDMM and RMM ($p<0.0001$ and $p=0.01$, resp., **Figure 4C**, **suppl. Figure S7**), in line with the observation of higher exposure to mutational signature AC3 in RRMM than in NDMM and RMM. In 6 of 39 RRMM samples, the HRDetect scores exceeded the value of 0.7, a cut-off which was recently established to identify tumors with a high level of BRCA1/BRCA2 deficiency.[26] Taken together, these observations indicate a shift in the activities of different mutational mechanisms during the course of the disease. This might be a consequence of mechanisms intrinsic to the tumor cells (e.g. acquisition of DNA repair deficiencies) or may result from exposure to therapeutic agents.

## Enriched chromosomal translocations in RRMM

Next, we sought to identify translocations, which were enriched or unique to RRMM (**Figure 5A**, **suppl. Figure 8**). While MYC rearrangements per se were not enriched in RRMM, *FAM46C-MYC* translocations (n=4) and local rearrangements of chr8q24.21 (n=4) were both found exclusively in RRMM patients (**Figure 5B**). The super-enhancer of *FAM46C* showed rearrangements involving a number of target genes such as the transcription factor and presumed oncogene *LMO4*. Analysis of expression data confirmed enhancer hijacking (**suppl. Figure S9**). IgH translocations involving *MYCN* were observed in two cases as part of composite t(4;14)-t(2;4) translocations also involving the *MMSET* locus, co-activating *MMSET* and *MYCN*. In these cases, *MYCN* was highly expressed, while *MYC* expression was completely suppressed (**suppl. Figure S10**). Both cases showed extramedullary disease, secondary plasma cell leukemia and a distinct plasmablastic cytological appearance. In one case, retrospective analysis of earlier samples revealed the absence of the secondary t(2;4)

translocation and absence of concomitant *MYCN* activation and *MYC* suppression, suggesting the emergence of *MYCN* overexpression with disease progression.

## Discussion

This comprehensive study of extensively pretreated, highly refractory MM by WGS and RNA-Seq suggests that the pathophysiology of NDMM and the biology of refractory disease are strikingly different. In RRMM, we observed marked genomic instability with impaired DNA repair mechanisms, in particular homologous recombination repair (HRR), which we confirmed using the well-established HRDetect algorithm. Mutational signatures indicative of impaired DNA repair, such as AC3, have been reported in NDMM although not to the extent observed here in this highly refractory setting.[32, 33] A recent study has reported the absence of mutational signature AC3 and HRR deficiency in NDMM and has classified the appearance of signature AC3 in NDMM as a false positive effect of the applied deconvolution method.[15] A study on the genomic make-up of relapsed but less heavily pretreated RMM using whole-exome sequencing did not report mutational signature AC3, but rather a novel signature associated with alkylator therapies.[13] In our work, we find both mutational signatures and thereby provide evidence that they are not reflective of the same underlying mutational process and can be deconvoluted with sufficient statistical power in the underlying data.

Walker *et al* recently used the term *double hit* MM to indicate a subset of NDMM with a very poor prognosis including patients with bi-allelic TP53 inactivation.[34] In our study, patients with a *TP53 double hit* experienced the worst outcomes in RRMM, confirming recent observations in the relapsed setting.[10, 35] Further genes with recurrent bi-allelic aberrations in RRMM include *RB1* and *TRAF3*, though they did not independently affect the prognosis in our cohort, likely attributable to the limited number of patients which had 'double hits' in these TSGs but without concomitant bi-allelic *TP53* events.

*BRAF* mutations occur at a higher prevalence in RRMM. The frequency seen in our cohort seems to even exceed those previously reported in RRMM,[36] a finding which may reflect the heavily pretreated

nature of the patient cohort presented here. However, a possible selection bias has to be kept in mind because a strong driver mutation like BRAF V600E might be associated with higher tumor load, thus potentially resulting in a higher success rate of plasma cell purification for WGS. Also, the limited sample size might have contributed to this finding. Nonetheless, the eight cases of the druggable mutation BRAF V600E are of particular therapeutic interest.[37, 38]

Among potential resistance-conferring SNVs, individual genes were only affected at low frequencies. However, at the level of functional networks, recurrence was actually seen. We found mutations in several proteasomal subunits as well as in TJP1 which modulates PI sensitivity in MM.[12, 30, 39] While the functional impact of most of these mutations remains to be proven, their enrichment in RRMM supports an association with PI resistance. The same holds true for mutations in genes presumably associated with IMiD resistance, such as *CRBN*, *CUL4B*, and *IZKF1*. Furthermore, we detected mutations in three members of the COP9 signalosome complex (COPS3, COPS4, and COPS8) and CAND1, further supporting their functional impact on IMiD activity.[31]

The increased mutational load might both explain the higher capacity of MM cells to adapt to treatment and facilitate the emergence of resistance. One of the mechanisms contributing to the higher mutational load in RRMM appears to be impaired DNA double-strand break HRR with the potential therapeutic implication of synthetic lethality to pharmacological inhibitors of DNA damage response, such as ATR inhibitors. At the same time, we found mutations in genes associated with sensitivity to PARP inhibitors in 49% of RRMM patients. This further strengthens the rationale for assessing the therapeutic efficacy of ATR and PARP inhibition in RRMM as has been shown, for example, in solid cancers with *BRCAness* characteristics.[40] In fact, there is plenty of pre-clinical evidence for synthetic lethality conferred by such inhibitors in MM cell lines with high rates of ongoing DNA damage.[41-43] As PI treatment has been suggested to induce a *BRCAness*-like state in MM cells via impairment of DNA repair pathways,[44] there may also be a rationale for combining PI and PARP inhibitors in MM. However, these concepts need to be confirmed within clinical trials.

One major limitation of our study is that comparative analyses were performed between independent NDMM, RMM, and RRMM patient cohorts, limiting the ability to draw conclusions as to the tumor evolution under treatment. Thus, one can only speculate as to whether genomic instability was pre-existing in these cases, e.g. restricted to certain focal lesions,[45] and was then selected for or whether it was newly acquired following treatment with e.g. DNA damaging drugs. Longitudinal analyses that also address spatial heterogeneity will therefore be of particular interest. While this real world RRMM cohort represents similarly ultra-refractory MM patients, the route taken to this end stage disease differed greatly between individual patients. It is well conceivable, that important biological differences exist between RRMM patients reaching refractoriness after multiple lines of treatment and those progressing fast through a limited number of therapies. Our RRMM cohort size might therefore be too small to overcome the heterogeneity of this patient population with sufficient statistical power. Further analyses on larger or more homogeneous RRMM patient cohorts will help elucidate these issues.

In conclusion, based on our observation that RRMM is characterized by marked genomic instability, which enables MM cells to rapidly adapt to selective therapeutic pressure, treatment strategies focused on exploiting impaired HRR should be evaluated within prospective clinical trials. Such strategies might be particularly useful in the current era of novel immunotherapies in MM as recent reports suggest genomic instability as a mechanism of resistance to CAR T cell treatment.[46, 47] Targeting impaired DNA repair mechanisms may therefore help to improve the outcomes of patients with RRMM.

## References

1. Kumar SK, Rajkumar SV, Dispenzieri A, et al. Improved survival in multiple myeloma and the impact of novel therapies. Blood. 2008;111(5):2516-2520.

2. Kumar SK, Lee JH, Lahuerta JJ, et al. Risk of progression and survival in multiple myeloma relapsing after therapy with IMiDs and bortezomib: a multicenter international myeloma working group study. Leukemia. 2012;26(1):149-157.

3. Kumar SK, Dimopoulos MA, Kastritis E, et al. Natural history of relapsed myeloma, refractory to immunomodulatory drugs and proteasome inhibitors: a multicenter IMWG study. Leukemia. 2017;31(11):2443-2448.

4. Usmani SZ, Weiss BM, Plesner T, et al. Clinical efficacy of daratumumab monotherapy in patients with heavily pretreated relapsed or refractory multiple myeloma. Blood. 2016;128(1):37-44.

5. Chapman MA, Lawrence MS, Keats JJ, et al. Initial genome sequencing and analysis of multiple myeloma. Nature. 2011;471(7339):467-472.

6. Walker BA, Boyle EM, Wardell CP, et al. Mutational Spectrum, Copy Number Changes, and Outcome: Results of a Sequencing Study of Patients With Newly Diagnosed Myeloma. J Clin Oncol. 2015;33(33):3911-3920.

7. Walker BA, Mavrommatis K, Wardell CP, et al. Identification of novel mutational drivers reveals oncogene dependencies in multiple myeloma. Blood. 2018;132(6):587-597.

8. Bolli N, Avet-Loiseau H, Wedge DC, et al. Heterogeneity of genomic evolution and mutational profiles in multiple myeloma. Nat Commun. 2014;5:2997.

9. Lohr JG, Stojanov P, Carter SL, et al. Widespread genetic heterogeneity in multiple myeloma: implications for targeted therapy. Cancer Cell. 2014;25(1):91-101.

10. Weinhold N, Ashby C, Rasche L, et al. Clonal selection and double-hit events involving tumor suppressor genes underlie relapse in myeloma. Blood. 2016;128(13):1735-1744.

11. Kortum KM, Mai EK, Hanafiah NH, et al. Targeted sequencing of refractory myeloma reveals a high incidence of mutations in CRBN and Ras pathway genes. Blood. 2016;128(9):1226-1233.

12. Barrio S, Stuhmer T, Da-Via M, et al. Spectrum and functional validation of PSMB5 mutations in multiple myeloma. Leukemia. 2019;33(2):447-456.

13. Zicchedda B, Biancon G, Bagnoli F, et al. Integrative analysis of the genomic and transcriptomic landscape of double-refractory multiple myeloma. Blood Adv. 2020;4(5):830-844.

14. Maura F, Bolli N, Angelopoulos N, et al. Genomic landscape and chronological reconstruction of driver events in multiple myeloma. Nat Commun. 2019;10(1):3835.

15. Maura F, Degasperi A, Nadeu F, et al. A practical guide for mutational signature analysis in hematological malignancies. Nat Commun. 2019;10(1):2969.

16. Paramasivam N, Hubschmann D, Toprak UH, et al. Mutational patterns and regulatory networks in epigenetic subgroups of meningioma. Acta Neuropathol. 2019;138(2):295-308.

17. Li H. Aligning sequence reads, clone sequences and assembly contigs with BWA-MEM. arXiv. 2013;1303.3997. [Preprint]

18. Tarasov A, Vilella AJ, Cuppen E, Nijman IJ, Prins P. Sambamba: fast processing of NGS alignment formats. Bioinformatics. 2015;31(12):2032-2034.

19. Rimmer A, Phan H, Mathieson I, et al. Integrating mapping-, assembly- and haplotype-based approaches for calling variants in clinical sequencing applications. Nat Genet. 2014;46(8):912-918.

20. Harrow J, Frankish A, Gonzalez JM, et al. GENCODE: the reference human genome annotation for The ENCODE Project. Genome Res. 2012;22(9):1760-1774.

21. Wang K, Li M, Hakonarson H. ANNOVAR: functional annotation of genetic variants from high-throughput sequencing data. Nucleic Acids Res. 2010;38(16):e164.

22. Gonzalez-Perez A, Perez-Llamas C, Deu-Pons J, et al. IntOGen-mutations identifies cancer drivers across tumor types. Nat Methods. 2013;10(11):1081-1082.

23. Hubschmann D, Jopp-Saile L, Andresen C, et al. Analysis of mutational signatures with yet another package for signature analysis. Genes Chromosomes Cancer. 2021;60(5):314-331.

24. Rustad EH, Yellapantula V, Leongamornlert D, et al. Timing the initiation of multiple myeloma. Nat Commun. 2020;11(1):1917.

25. Lopez C, Kleinheinz K, Aukema SM, et al. Genomic and transcriptomic changes complement each other in the pathogenesis of sporadic Burkitt lymphoma. Nat Commun. 2019;10(1):1459.

26. Davies H, Glodzik D, Morganella S, et al. HRDetect is a predictor of BRCA1 and BRCA2 deficiency based on mutational signatures. Nat Med. 2017;23(4):517-525.

27. Zhao EY, Shen Y, Pleasance E, et al. Homologous Recombination Deficiency and Platinum-Based Therapy Outcomes in Advanced Breast Cancer. Clin Cancer Res. 2017;23(24):7521-7530.

28. Dobin A, Davis CA, Schlesinger F, et al. STAR: ultrafast universal RNA-seq aligner. Bioinformatics. 2013;29(1):15-21.

29. Heining C, Horak P, Uhrig S, et al. NRG1 Fusions in KRAS Wild-Type Pancreatic Cancer. Cancer Discov. 2018;8(9):1087-1095.

30. Zhang XD, Baladandayuthapani V, Lin H, et al. Tight Junction Protein 1 Modulates Proteasome Capacity and Proteasome Inhibitor Sensitivity in Multiple Myeloma via EGFR/JAK1/STAT3 Signaling. Cancer Cell. 2016;29(5):639-652.

31. Sievers QL, Gasser JA, Cowley GS, Fischer ES, Ebert BL. Genome-wide screen identifies cullin-RING ligase machinery required for lenalidomide-dependent CRL4(CRBN) activity. Blood. 2018;132(12):1293-1303.

32. Hoang PH, Cornish AJ, Dobbins SE, Kaiser M, Houlston RS. Mutational processes contributing to the development of multiple myeloma. Blood Cancer J. 2019;9(8):60.

33. Hoang PH, Dobbins SE, Cornish AJ, et al. Whole-genome sequencing of multiple myeloma reveals oncogenic pathways are targeted somatically through multiple mechanisms. Leukemia. 2018;32(11):2459-2470.

34. Walker BA, Mavrommatis K, Wardell CP, et al. A high-risk, Double-Hit, group of newly diagnosed myeloma identified by genomic analysis. Leukemia. 2019;33(1):159-170.

35. Lakshman A, Painuly U, Rajkumar SV, et al. Impact of acquired del(17p) in multiple myeloma. Blood Adv. 2019;3(13):1930-1938.

36. Xu J, Pfarr N, Endris V, et al. Molecular signaling in multiple myeloma: association of RAS/RAF mutations and MEK/ERK pathway activation. Oncogenesis. 2017;6(5):e337.

37. Andrulis M, Lehners N, Capper D, et al. Targeting the BRAF V600E mutation in multiple myeloma. Cancer Discov. 2013;3(8):862-869.

38. Raab MS, Lehners N, Xu J, et al. Spatially divergent clonal evolution in multiple myeloma: overcoming resistance to BRAF inhibition. Blood. 2016;127(17):2155-2157.

39. Shi CX, Kortum KM, Zhu YX, et al. CRISPR Genome-Wide Screening Identifies Dependence on the Proteasome Subunit PSMC6 for Bortezomib Sensitivity in Multiple Myeloma. Mol Cancer Ther. 2017;16(12):2862-2870.

40. Lord CJ, Ashworth A. BRCAness revisited. Nat Rev Cancer. 2016;16(2):110-120.

41. Cottini F, Hideshima T, Suzuki R, et al. Synthetic Lethal Approaches Exploiting DNA Damage in Aggressive Myeloma. Cancer Discov. 2015;5(9):972-987.

42. Herrero AB, Gutierrez NC. Targeting Ongoing DNA Damage in Multiple Myeloma: Effects of DNA Damage Response Inhibitors on Plasma Cell Survival. Front Oncol. 2017;7:98.

43. Botrugno OA, Bianchessi S, Zambroni D, et al. ATR addiction in multiple myeloma: synthetic lethal approaches exploiting established therapies. Haematologica. 2020;105(10):2440-2447.

44. Neri P, Ren L, Gratton K, et al. Bortezomib-induced "BRCAness" sensitizes multiple myeloma cells to PARP inhibitors. Blood. 2011;118(24):6368-6379.

45. Rasche L, Chavan SS, Stephens OW, et al. Spatial genomic heterogeneity in multiple myeloma revealed by multi-region sequencing. Nat Commun. 2017;8(1):268.

46. Orlando EJ, Han X, Tribouley C, et al. Genetic mechanisms of target antigen loss in CAR19 therapy of acute lymphoblastic leukemia. Nat Med. 2018;24(10):1504-1506.

47. Da Via MC, Dietrich O, Truger M, et al. Homozygous BCMA gene deletion in response to anti-BCMA CAR T cells in a patient with multiple myeloma. Nat Med. 2021;27(4):616-619.

## Figure legends

**Figure 1. High genomic complexity and mutational load in RRMM vs NDMM.**

**A. SV and SNV load per patient in RRMM vs NDMM.**

SNV and SV counts are plotted for each patient in both cohorts showing a higher overall mutational load in RRMM (blue) vs NDMM (red). Each dot represents an individual patient. The example cases shown in panels C and D are annotated as RRMM_16 and RRMM_15, respectively.

**B. Differences in SV types in RRMM vs NDMM.**

Median and range of number of overall SVs per patient in RRMM (blue) vs NDMM (red) are shown as well as deletions (DEL), duplications (DUP), inversions (INV), and translocations (TRA).

**C. Example case of RRMM displaying chromoplexy.**

Green lines represent translocations, blue lines deletions, red lines duplications, and black lines inversions. Transparency of lines is based on estimated SV clonality. Variant existence is represented by bar plots. The outer layer represents copy number variations and display the copy-neutral nature of the chromoplexy event.

**D. Example case of RRMM displaying chromothripsis.**

Green lines represent translocations, blue lines deletions, red lines duplications, and black lines inversions. Transparency of lines is based on estimated SV clonality. Variant existence is represented by bar plots. The outer layer represents copy number variations.

**E. Genome-wide small variant mutational load in RRMM vs NDMM.**

The number of mutations per patients and length of genome in megabases (MB) is shown in RRMM (blue) vs NDMM (red).

**F. Genomic instability scores in RRMM vs NDMM.**

The unbiased sum of HRD, LST, and TAI scores is shown for RRMM (blue) vs NDMM (red) illustrating a higher genomic instability in RRMM.

To compensate for differing sequencing depths in both cohorts, the RRMM dataset was subsampled for these analyses.

**Figure 2. Significantly mutated driver genes in RRMM.** Significantly mutated drivers and their prevalence in the RRMM cohort are shown as well as copy number aberrations (CNAs) of chromosome arms 13q, 1q, 17p, 1p, presence or absence of hyperdiploid karyotype, and the genomic instability score.

**Figure 3. Impact of TP53 alteration on PFS (A) and OS (B) in RRMM.** PFS and OS is shown for RRMM patients with a bi-allelic event involving the TP53 locus (red), a mono-allelic event (blue) or no event (black) illustrating the inferior outcome of patients with bi-allelic TP53 aberrations. PFS and OS were calculated from time of sampling.

**Figure 4. Exposure to mutational signatures in RRMM vs RMM vs NDMM patients.**

A. **Absolute exposure to mutational signatures in RRMM vs RMM vs NDMM patients.**
   Exposure to mutational signatures based on the Alexandrov COSMIC (AC) catalogue with the addition of the MM1 signature recently linked to melphalan exposure is shown for RRMM (blue) vs RMM (green) vs NDMM (red) patients. Most notable is an increased impact of signatures AC3 (light brown) and MM1 (black) in RRMM.
B. **Relative exposure to mutational signatures in RRMM vs RMM vs NDMM patients.**
   Exposure to mutational signatures is shown for RRMM (blue) vs RMM (green) vs NDMM (red) patient cohorts. Significant differences in exposure are indicated with the following p-values: * <0.05, ** <0.01, *** < 0.001. Most notable is a significant increase of signature AC3 in RRMM compared to NDMM and RMM as well as a significant step-wise increase of signature MM1 in RRMM vs RMM vs NDMM.
C. **HRDetect scores in RRMM vs RMM vs NDMM patients.**
   HRDetect scores in RRMM (blue) vs RMM (green) vs NDMM (red) indicate a significant increase in impaired homologous recombination repair features in RRMM.

To compensate for differing sequencing depths in both cohorts, the RRMM dataset was subsampled for this analysis.

**Figure 5. Immunoglobulin translocations and MYC rearrangements in RRMM.**

**A. Immunoglobulin translocations in RRMM.**

Translocations involving the immunoglobulin heavy chain (IGH) locus, the lambda light chain (IGL), and the kappa light chain (IGK) locus are shown. The number of patients with involvement of the respective partner genes are given in brackets. Patient RRMM_34 harboring a very complex IGL translocation was excluded from this graph for reasons of readability and is shown separately in **suppl. Figure S8**. Cytobands, chromosome arms and chromosomes were also stretched and compressed to emphasize targets of immunoglobulin translocations and to improve readability.

**B. MYC rearrangements in RRMM.**

Most notable are local rearrangements as well as those involving the IGL locus or FAM46C.

Orange lines represent immunoglobulin locus translocations, purple lines secondary immunoglobulin locus related translocations. Secondary translocations of the immunoglobulin loci were defined as secondary events with one of the breakpoints of the SV not further away than 2MB from the target breakpoint of a given primary immunoglobulin translocation (i.e. IG —PrimarySV—> PrimaryTarget —SecondarySV—>SecondaryTarget). Green lines indicate non-IG locus translocations, blue lines deletions, red lines duplications, and black lines inversions.

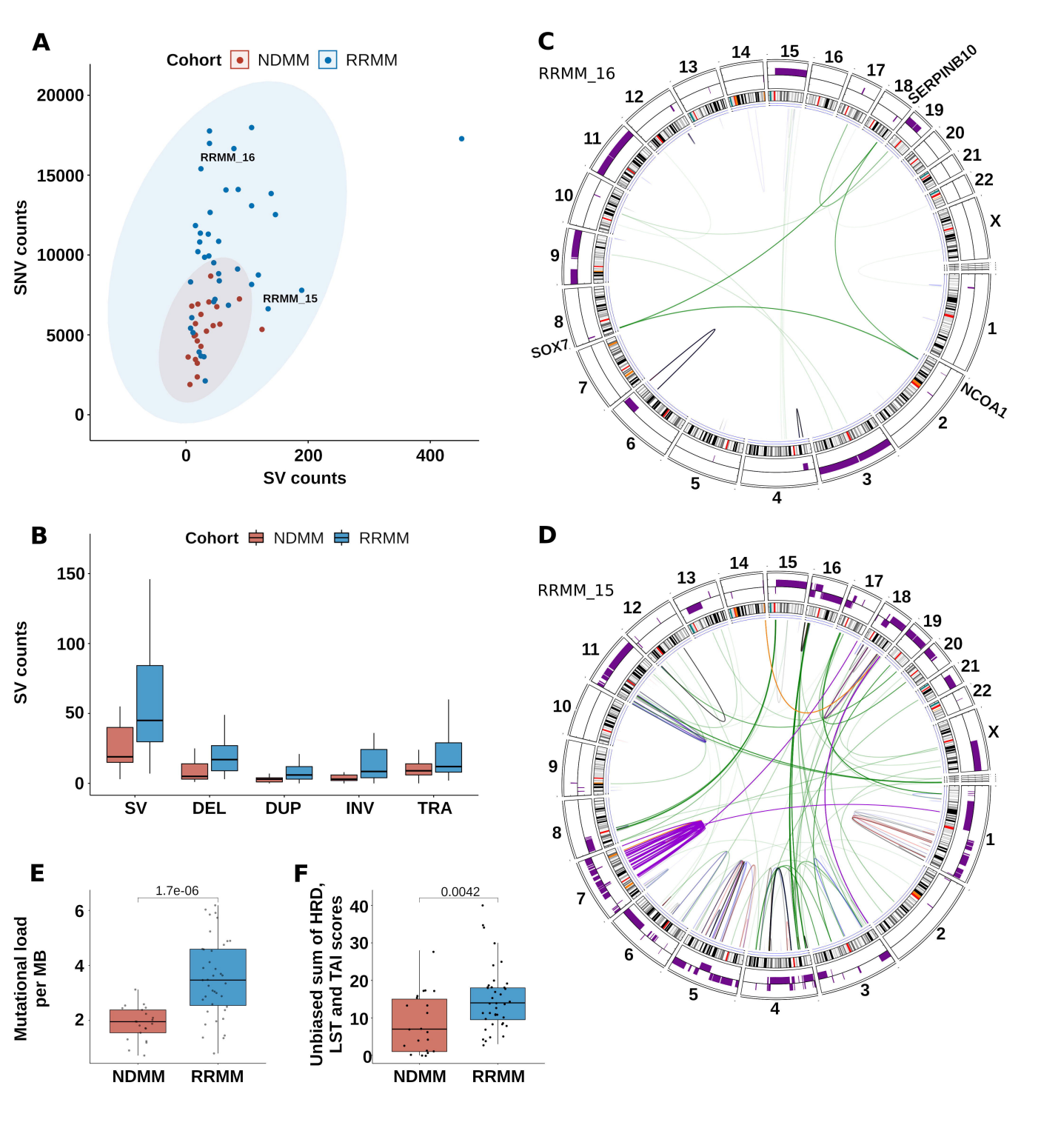
A
Cohort NDMM RRMM
SNV counts
SV counts
RRMM_16
RRMM_15
B
Cohort NDMM RRMM
SV counts
SV
DEL
DUP
INV
TRA
C
RRMM_16
SERPINB10
SOX7
NCOA1
D
RRMM_15
E
Mutational load per MB
1.7e-06
NDMM
RRMM
F
Unbiased sum of HRD, LST and TAI scores
0.0042
NDMM
RRMM

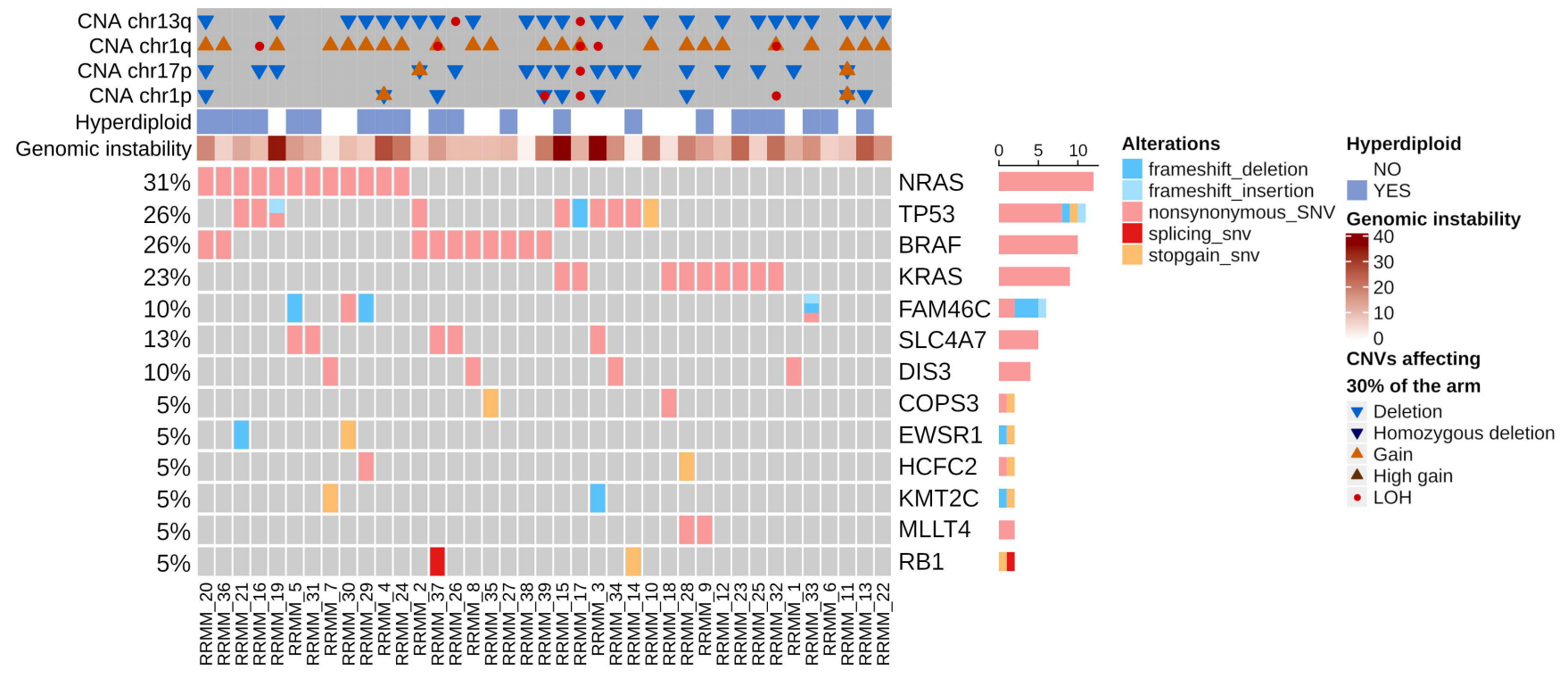
CNA chr13q
CNA chr1q
CNA chr17p
CNA chr1p
Hyperdiploid
Genomic instability
31%
26%
26%
23%
10%
13%
10%
5%
5%
5%
5%
5%
5%
NRAS
TP53
BRAF
KRAS
FAM46C
SLC4A7
DIS3
COPS3
EWSR1
HCFC2
KMT2C
MLLT4
RB1
0
5
10
RRMM_20
RRMM_36
RRMM_21
RRMM_16
RRMM_19
RRMM_5
RRMM_31
RRMM_7
RRMM_30
RRMM_29
RRMM_4
RRMM_24
RRMM_2
RRMM_37
RRMM_26
RRMM_8
RRMM_35
RRMM_27
RRMM_38
RRMM_39
RRMM_15
RRMM_17
RRMM_3
RRMM_34
RRMM_14
RRMM_10
RRMM_18
RRMM_28
RRMM_9
RRMM_12
RRMM_23
RRMM_25
RRMM_32
RRMM_1
RRMM_33
RRMM_6
RRMM_11
RRMM_13
RRMM_22
Alterations
frameshift_deletion
frameshift_insertion
nonsynonymous_SNV
splicing_snv
stopgain_snv
Hyperdiploid
NO
YES
Genomic instability
40
30
20
10
0
CNVs affecting
30% of the arm
Deletion
Homozygous deletion
Gain
High gain
LOH

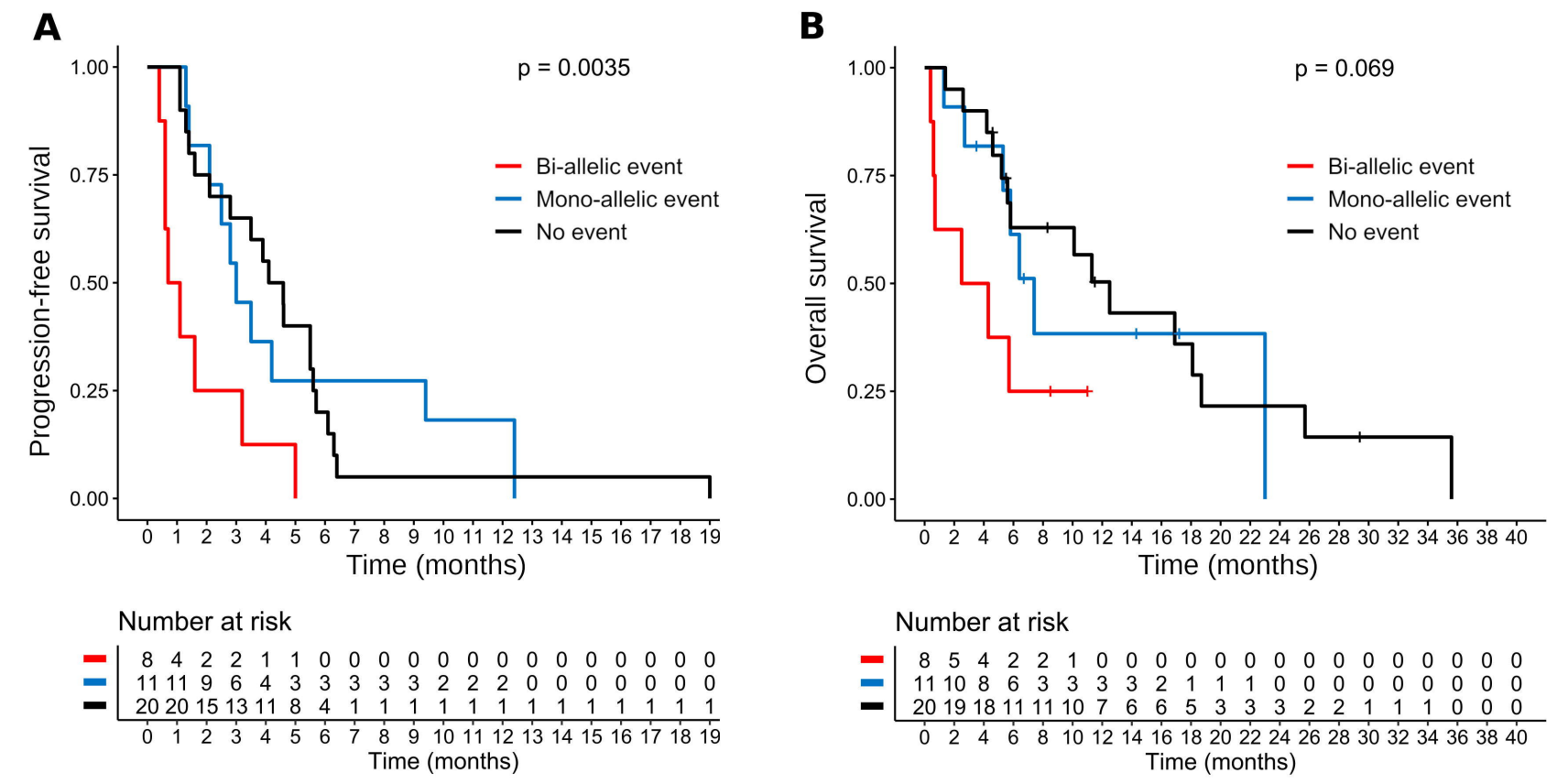
A
Progression-free survival
1.00
0.75
0.50
0.25
0.00
p = 0.0035
Bi-allelic event
Mono-allelic event
No event
0 1 2 3 4 5 6 7 8 9 10 11 12 13 14 15 16 17 18 19
Time (months)
Number at risk
8 4 2 2 1 1 0 0 0 0 0 0 0 0 0 0 0 0 0 0
11 11 9 6 4 3 3 3 3 3 2 2 2 0 0 0 0 0 0 0
20 20 15 13 11 8 4 1 1 1 1 1 1 1 1 1 1 1 1 1
0 1 2 3 4 5 6 7 8 9 10 11 12 13 14 15 16 17 18 19
Time (months)
B
Overall survival
1.00
0.75
0.50
0.25
0.00
p = 0.069
Bi-allelic event
Mono-allelic event
No event
0 2 4 6 8 10 12 14 16 18 20 22 24 26 28 30 32 34 36 38 40
Time (months)
Number at risk
8 5 4 2 2 1 0 0 0 0 0 0 0 0 0 0 0 0 0 0 0
11 10 8 6 3 3 3 3 2 1 1 1 0 0 0 0 0 0 0 0 0
20 19 18 11 11 10 7 6 6 5 3 3 3 2 2 1 1 1 0 0 0
0 2 4 6 8 10 12 14 16 18 20 22 24 26 28 30 32 34 36 38 40
Time (months)

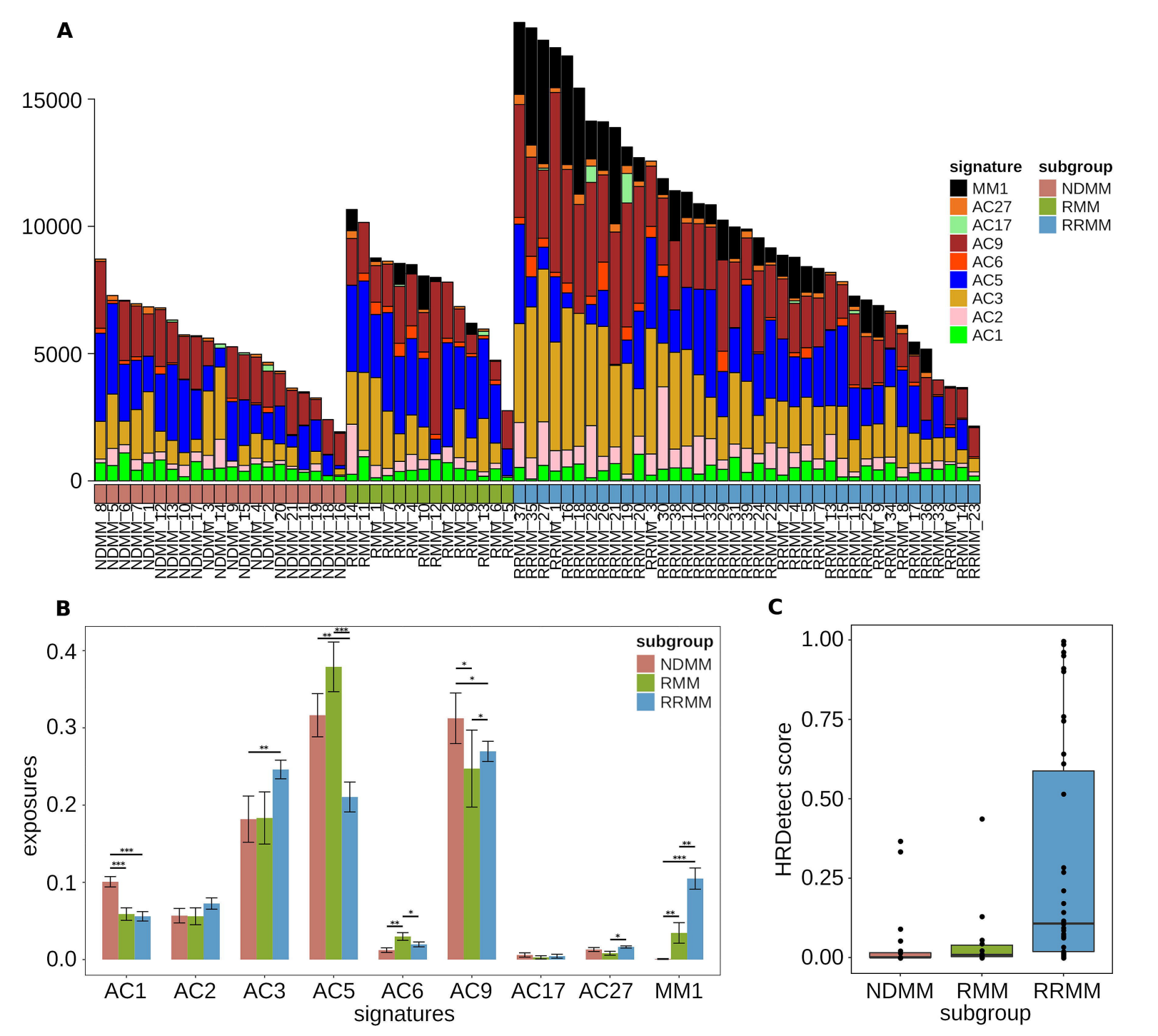
A
15000
10000
5000
0
signature
MM1
AC27
AC17
AC9
AC6
AC5
AC3
AC2
AC1
subgroup
NDMM
RMM
RRMM
B
exposures
0.4
0.3
0.2
0.1
0.0
subgroup
NDMM
RMM
RRMM
AC1
AC2
AC3
AC5
AC6
AC9
AC17
AC27
MM1
signatures
C
HRDetect score
1.00
0.75
0.50
0.25
0.00
NDMM
RMM
RRMM
subgroup

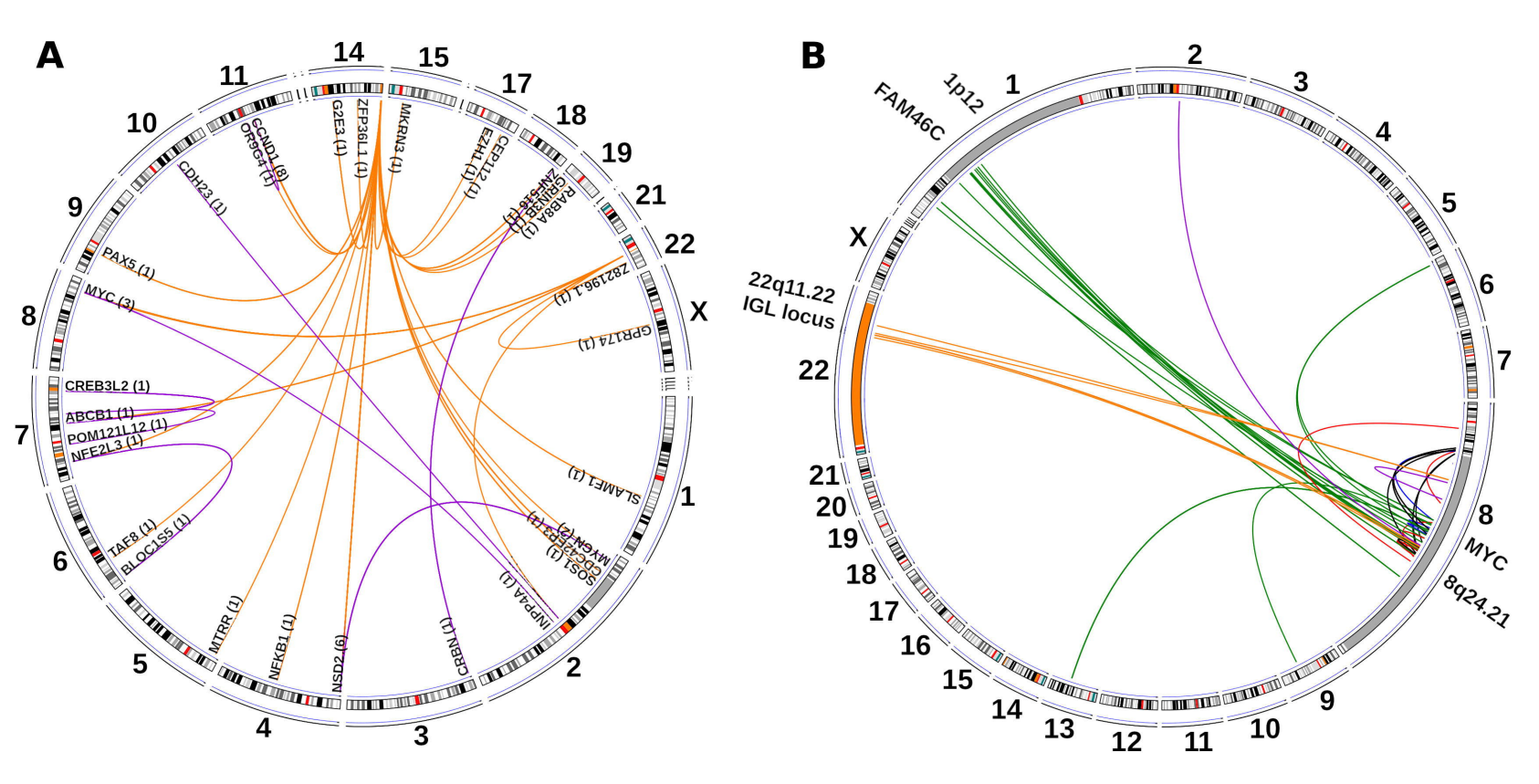
A
B
FAM46C
1p12
22q11.22
IGL locus
MYC
8q24.21
CDH23 (1)
PAX5 (1)
MYC (3)
CREB3L2 (1)
ABCB1 (1)
POM121L12 (1)
NFE2L3 (1)
TAF8 (1)
BLOC1S5 (1)
MTRR (1)
NFKB1 (1)
NSD2 (6)
CARNLI (1)
INPP4A (1)
SOS1 (1)
MXI1 (2)
SLAMF1 (1)
GPR174 (1)
Z82196.1 (1)
RABBA (1)
ZNF318 (1)
CEP112 (1)
EZH1 (1)
MKRN3 (1)
ZFP36L1 (1)
G2E3 (1)
OR9G4 (1)
GCNA1 (8)

# Supplementary Information

## *Supplementary Methods*

### Alignment of RRMM and NDMM

The raw reads were mapped to the human reference genome (build 37, version hs37d5), using BWA mem[1] (version 0.7.8, with parameter -T 0). A Phi X 174 contig (NC_001422.1) was added to the reference genome to remove the Phi X spike-in used during the sequencing. The mapped reads were sorted using SAMtools[2] (version 0.1.19), and lanes were merged and duplicate reads were marked using Sambamba[3] (version 0.5.9, with parameter -t 6 -l 9 --hash-table-size=2000000 --overflow-list-size=1000000 --io-buffer-size=64). Similar alignment workflow and parameters were applied to the raw reads from NDMM samples except that the BWA and Sambamba version were updated to 0.7.15 and 0.6.5 respectively.

To assess the effect of differing sequencing depths between the NDMM, RMM and RRMM samples on variant calling, subsampling of RRMM samples was performed using Sambamba (version 0.6.6, with parameters view -h -t 20 -s 0.5 -f bam --subsampling-seed=42) to achieve a 50% lower coverage which was comparable to the coverage of the set of NDMM (**suppl. Figure S1, S2**).

### Small variant calling

SNVs and indels were called using in-house pipelines developed for the ICGC Pan-Cancer Analysis of Whole Genomes (PCAWG) project.[4] Briefly, SNVs were called in tumor samples using SAMtools mpileup (version 0.1.19, with parameters -REI -q 30 -ug) and bcftools view (with parameters -vcgN -p 2.0). We have disabled the Bayesian model in bcftools (by setting -p 2.0), which allows calling low variant allele frequency (VAF) variants. In the next step each of these variant positions were queried in the control sample using SAMtools mpileup (with parameters -ABRI -Q 0 -q 1). Variants were further annotated with Gencode[5] (version 19) and ANNOVAR[6]; 1000 genome variants, dbSNP variants and variant frequency from our local control were further annotated. Somatic variant classification and

confidence scores (with range 1 to 10) were added as described previously,[7] and variants with a score of 8 and above were considered as high confidence variants.

Indels were called together in control and tumor samples using Platypus[8] (version 0.8.1, with parameters -bufferSize = 100,000 -maxReads = 5,000,000) and gene definitions and databases were annotated similar to SNVs. As described previously,[9] somatic SNVs and indels present in ten or more samples in our local control database consisting of 280 WGS control samples from different cohorts, which were processed using the same pipelines, were considered as technical artifacts and were removed.

Further Combined Annotation Dependent Depletion (CADD) scores (version 1.3) were added to the variants.

Somatic small variants misclassified as germline variant due to contamination of normal control samples with tumor cell DNA were rescued using our in-house tool TiNDA, which uses the EM-algorithm implemented in Canopy[10] (version 1.2.0) to cluster variants based on VAFs. Clusters in which at least 85% of variants have a higher VAF in tumor compared to control and 85% of the variants have VAF below 0.45 in control and above 0.01 in tumor were considered as somatic clusters. Rescued variants with high confidence scores were merged with the remaining high confidence somatic variants.

Significance of subgroup differences (NDMM vs. RRMM) regarding mutational load were assessed by the Wilcoxon rank sum test.

The merged set of variants was used to identify driver genes using IntOGen[11] (version 3.0.5) with the parameters: --split-size 5000; with configuration: 'significance_threshold' as 0.1 for oncodrivefm, oncodriveclust and mutsig, 'samples_threshold' as 2 and 5 for oncodrivefm and oncodriveclst respectively. The identified driver genes were used to generate the oncoprint using ComplexHeatmap[12]. Significance of subgroup differences (NDMM vs. RRMM) regarding prevalences of gene mutations were assessed by Fisher's exact test.

## Supervised analysis of mutational signatures

A supervised analysis of mutational signatures was performed with the R package YAPSA.[13] The function LCD_complex_cutoff() in YAPSA was used to compute a non-negative least square (NNLS) decomposition of the mutational catalogue with the 30 known signatures from COSMIC v2 (https://cancer.sanger.ac.uk/signatures/signatures_v2/). To unambiguously identify the used signature set we denominate these signatures as AC1–AC30 (as abbreviation for Alexandrov COSMIC). The MM1 signature which was recently linked to melphalan exposure was added.[14, 15] After a first NNLS decomposition, the computed exposures are compared to optimal signature-specific cutoffs in order to reduce false positive calls, and then only those signatures whose exposures are higher than these signature-specific cutoffs are kept for the analysis and fed into a second NNLS decomposition yielding the final exposures. YAPSA was also used for stratified analysis of mutational signatures in order to identify enrichment and depletion patterns. Breakpoint proximity was used as stratification axis with three strata: vicinity (distance to closest breakpoint < 100 kbp), intermediate (distance to closest breakpoint between 100 kbp and 1 Mbp), and background (distance to closest breakpoint > 1 Mbp). Significance of enrichment and depletion patterns as well as of subgroup differences (NDMM vs. RRMM) were assessed by the Kruskal Wallis test and if that revealed significance in more than two groups, Nemenyi tests were performed as post-hoc tests.

## Identification of Kataegis clusters

As outlined previously,[16] we defined Kataegis-like clusters to be regions of increased SNV density with at least five SNVs with at most 1000 bp intermutational distance in one sample, similar to what has previously been defined as Kataegis.[17] We defined a Kataegis cluster to be recurrent if it was found in at least three samples, i.e., if in three samples Kataegis clusters were identified with a minimal region of overlap. Differences in the number of Kataegis clusters and in the prevalence of SNV location within and outside of Kataegis clusters in RRMM vs NDMM were assessed by Wilcoxon rank sum tests.

## Structural variants

Structural variants (SVs) were detected using the DKFZ SOPHIA workflow version 2.0.2 available in https://github.com/DKFZ-ODCF/SophiaWorkflow with the source code of the SOPHIA algorithm available in https://bitbucket.org/utoprak/sophia/.[9, 16] SOPHIA is an SV detection algorithm incorporating discordant mate, split read and a background breakpoint database from 3417 blood samples of donors from published international and ongoing internal DKFZ projects. The data in the background breakpoint database is obtained from sequencing results across the 101bp Illumina Hiseq2000/2500 and 151bp Illumina Hiseq X-Ten technologies. The SV candidate detection is a process of split-read and discordant mate evidence collection across each breakpoint as precursors for a SV, and SV candidates (pairs of breakpoints) are filtered by a complex decision tree trained by expert assessment of orthogonal FISH data. Secondary translocations of the immunoglobulin loci were defined as secondary events with one of the breakpoints of the SV not further away than 2MB from the target breakpoint of a given primary immunoglobulin translocation (i.e. IG —PrimarySV—> PrimaryTarget —SecondarySV—>SecondaryTarget).

For the statistical comparison of NDMM and RRMM with respect to SV types, only SVs with discordant mate support were considered in order to exclude the influences of different WGS libraries used in the two projects executed in different sequencing centers. Discordance in terms of mate distance was defined as a mate distance more than 5*MedianInsertSize or mate read mapping to a different chromosome. This typically limits the scope of the comparison to SVs with sizes $\gtrsim$1000bps.

Comparison of SV counts between the RRMM and NDMM cohorts was made using the Kruskal-Wallis test. Chromoplexy and chromothripsis statuses were assigned by manual visual inspection of SV calls and copy-number profiles on CIRCOS plots.

## Copy number variation detection

As described previously,[9, 16] copy number states were called and estimation of tumor purity and ploidy was performed using ACEseq (allele-specific copy number estimation from sequencing;

https://www.biorxiv.org/content/early/2017/10/29/210807). Structural variants called with SOPHIA were incorporated to improve genome segmentation. In cases where ACEseq provided multiple solutions for purity and ploidy, we manually selected the lowest ploidy solution which allowed to fit the majority of genomic segments to integer copy numbers and which also was consistent with the mutant allele frequency distribution of somatic SNVs. With regard to the TP53 containing region ACEseq plots were in addition inspected manually.

If at least 30% length of a chromosome arm or cytoband was affected by a CNV in a sample, then it was considered as chromosome arm-level or cytoband-level event for the sample. These sample level counts were used to find cytoband-level events that significantly differ between NDMM and RRMM cohorts. Significance of subgroup differences (NDMM vs. RRMM) were assessed by Fisher's exact test.

## Calculation of measures of genomic instability

First, genome copy number data from ACEseq was smoothed to prevent artificially elevated genomic instability measures due to oversegmentation caused by technical noise. To this end, segments for which allele-specific copy numbers did not deviate by more than 0.3 from each other were merged. Furthermore, segments smaller than 3 Mb were merged to the more similar neighboring segment as previously described.[18] Additionally, in the same chromosome, when the segments in p-arm extend into the centromeric region and start within the centromeric region in the q-arm, the segments were merged. These smoothed and merged segments were used to calculate the homologous recombination deficiency (HRD) score[18] and the number of large-scale transitions (LST) as previously described.[19] Briefly, segments larger than 15 Mb that were less than a whole chromosome in length and corresponded to a loss of heterozygosity were counted for the HRD score. For the quantification of LSTs, breaks between segments of different total copy number were counted with the constraint that both segments had to be larger than 10 Mb but did not correspond to entire chromosome arms. In addition, the telomeric-allelic imbalance (TAI) score,[20] which corresponds to the number of chromosomal segments with minimum length of 11MB and allelic imbalance extending into the subtelomeric regions, was calculated using the smoothed ACEseq results.[21] Genomic instability was

quantified as the sum of HRD, LST, and TAI scores. Significance of subgroup differences (NDMM vs. RRMM) were assessed by the Wilcoxon rank sum test.

## RNA sequencing

The paired-end reads were mapped to the STAR index generated reference genome (build 37, version hs37d5) using STAR[22] (version 2.5.2b). Genes' exons were defined by the GENCODE v19 gene models.[5] The gene expressions were quantified using featureCounts (Subread version 1.5.1). For differential gene expression analysis and detection of enhancer hijacking, raw read counts were normalized by a preliminary Counts Per Million (CPM) application where genes with less than 1 CPM were discarded from further analyses. Filtered gene read counts were normalized using the TMM method of the edgeR R package.[23, 24] TMM-normalized read counts were finalized by application of CPM and log2(x+1).

## Gene fusions

Gene fusions were detected using Arriba version 1.0.0 (https://github.com/suhrig/arriba) as described previously.[25] To further enrich for high-confidence fusion predictions, events involving genes marked as putative by the gene model or events with fewer supporting reads than 1 % of the local coverage (<5 % for read-through fusions) were discarded.

## References

1. Li H. Aligning sequence reads, clone sequences and assembly contigs with BWA-MEM. arXiv. 2013:1303.3997.

2. Li H, Handsaker B, Wysoker A, et al. The Sequence Alignment/Map format and SAMtools. Bioinformatics. 2009;25(16):2078-9.

3. Tarasov A, Vilella AJ, Cuppen E, Nijman IJ, Prins P. Sambamba: fast processing of NGS alignment formats. Bioinformatics. 2015;31(12):2032-4.

4. Consortium ITP-CAoWG. Pan-cancer analysis of whole genomes. Nature. 2020;578(7793):82-93.

5. Harrow J, Frankish A, Gonzalez JM, et al. GENCODE: the reference human genome annotation for The ENCODE Project. Genome Res. 2012;22(9):1760-74.

6. Wang K, Li M, Hakonarson H. ANNOVAR: functional annotation of genetic variants from high-throughput sequencing data. Nucleic acids research. 2010;38(16):e164.

7. Jones DT, Hutter B, Jager N, et al. Recurrent somatic alterations of FGFR1 and NTRK2 in pilocytic astrocytoma. Nature genetics. 2013;45(8):927-32.

8. Rimmer A, Phan H, Mathieson I, et al. Integrating mapping-, assembly- and haplotype-based approaches for calling variants in clinical sequencing applications. Nature genetics. 2014;46(8):912-8.

9. Paramasivam N, Hubschmann D, Toprak UH, et al. Mutational patterns and regulatory networks in epigenetic subgroups of meningioma. Acta Neuropathol. 2019;138(2):295-308.

10. Jiang Y, Qiu Y, Minn AJ, Zhang NR. Assessing intratumor heterogeneity and tracking longitudinal and spatial clonal evolutionary history by next-generation sequencing. Proceedings of the National Academy of Sciences of the United States of America. 2016;113(37):E5528-37.

11. Gonzalez-Perez A, Perez-Llamas C, Deu-Pons J, et al. IntOGen-mutations identifies cancer drivers across tumor types. Nat Methods. 2013;10(11):1081-2.

12. Gu Z, Eils R, Schlesner M. Complex heatmaps reveal patterns and correlations in multidimensional genomic data. Bioinformatics. 2016;32(18):2847-9.

13. Hubschmann D, Jopp-Saile L, Andresen C, et al. Analysis of mutational signatures with yet another package for signature analysis. Genes Chromosomes Cancer. 2021;60(5):314-31.

14. Rustad EH, Yellapantula V, Leongamornlert D, et al. Timing the initiation of multiple myeloma. Nature communications. 2020;11(1):1917.

15. Maura F, Degasperi A, Nadeu F, et al. A practical guide for mutational signature analysis in hematological malignancies. Nature communications. 2019;10(1):2969.

16. Lopez C, Kleinheinz K, Aukema SM, et al. Genomic and transcriptomic changes complement each other in the pathogenesis of sporadic Burkitt lymphoma. Nature communications. 2019;10(1):1459.

17. Alexandrov LB, Nik-Zainal S, Wedge DC, et al. Signatures of mutational processes in human cancer. Nature. 2013;500(7463):415-21.

18. Abkevich V, Timms KM, Hennessy BT, et al. Patterns of genomic loss of heterozygosity predict homologous recombination repair defects in epithelial ovarian cancer. British journal of cancer. 2012;107(10):1776-82.

19. Popova T, Manie E, Rieunier G, et al. Ploidy and large-scale genomic instability consistently identify basal-like breast carcinomas with BRCA1/2 inactivation. Cancer research. 2012;72(21):5454-62.

20. Birkbak NJ, Wang ZC, Kim JY, et al. Telomeric allelic imbalance indicates defective DNA repair and sensitivity to DNA-damaging agents. Cancer discovery. 2012;2(4):366-75.

21. Brok WDd, Schrader KA, Sun S, et al. Homologous Recombination Deficiency in Breast Cancer: A Clinical Review. JCO Precision Oncology. 2017(1):1-13.

22. Dobin A, Davis CA, Schlesinger F, et al. STAR: ultrafast universal RNA-seq aligner. Bioinformatics. 2013;29(1):15-21.

23. Robinson MD, Oshlack A. A scaling normalization method for differential expression analysis of RNA-seq data. Genome Biol. 2010;11(3):R25.

24. Robinson MD, McCarthy DJ, Smyth GK. edgeR: a Bioconductor package for differential expression analysis of digital gene expression data. Bioinformatics. 2010;26(1):139-40.

25. Heining C, Horak P, Uhrig S, et al. NRG1 Fusions in KRAS Wild-Type Pancreatic Cancer. Cancer discovery. 2018;8(9):1087-95.

## *Supplementary Figure legends*

**Suppl. Figure S1. RRMM original data vs RRMM subsampled data vs NDMM for graphs presented in main figure 1, analysis of Copy number variants in NDMM and RRMM patients, and Kataegis and SNV distribution in RRMM vs NDMM.**

A. SV and SNV load per patient in RRMM original vs RRMM subsampled vs NDMM. SNV and SV counts are plotted for each patient showing a higher overall mutational load in RRMM, both the original data (orange) and the subsampled dataset (blue), vs NDMM (red). Each dot represents an individual patient. The example cases shown in main Figure 1, panels C and D, are annotated as RRMM_16 and RRMM_15, respectively.
B. Differences in SV types in RRMM original vs RRMM subsampled vs NDMM. Median and range of number of overall SVs per patient in RRMM, both original data (orange) and subsampled dataset (blue), vs NDMM (red) are shown as well as deletions (DEL), duplications (DUP), inversions (INV), and translocations (TRA).
C. Genome-wide small variant mutational load in RRMM original vs RRMM subsampled vs NDMM. The number of mutations per patients and length of genome in megabases (MB) is shown in RRMM, both original data (orange) and subsampled dataset (blue), vs NDMM (red).
D. Genomic instability scores in RRMM original vs RRMM subsampled vs NDMM. The unbiased sum of HRD, LST, and TAI scores is shown for RRMM, both original data (orange) and subsampled dataset (blue), vs NDMM (red) illustrating a higher genomic instability in RRMM.
E. Analysis of Copy number variants in NDMM and RRMM patients. Overview of somatic copy number aberrations (SCNAs) in NDMM vs RRMM patients. Orange indicates gain, blue indicates loss, red indicates loss of heterozygosity.
F. Recurrent regions of Kataegis in RRMM (blue) and NDMM (red) excluding the immunoglobulin loci. To compensate for differing sequencing depths in both cohorts, the RRMM dataset was subsampled for these analyses.

G. Kataegis and SNV distribution in RRMM vs NDMM. To compensate for differing sequencing depths in both cohorts, the RRMM dataset was subsampled for these analyses.

**Suppl. Figure S2. RNA expression (A) and prediction of functional relevance by CADD score (B) of significant driver genes in RRMM.**

A. Expression of small variants detected in significant driver genes in RRMM is indicated by variant allele frequency (VAF) in RNA sequencing with each dot representing an individual variant.
B. Prediction of functional relevance of small variants detected in significant driver genes in RRMM is indicated by Combined Annotation Dependent Depletion (CADD) score with each dot representing an individual variant. A CADD score > 20 indicates likely deleteriousness of the variant.

**Suppl. Figure S3. Mutational frequency in gene groups/networks NDMM vs RRMM.**

The prevalence of functional mutations in the following gene groups or networks in NDMM (red) vs RRMM (blue) is shown in the upper panel from left to right: genes associated with resistance to IMiDs, epigenetic modifiers, MAPK pathway, NFKB signaling, resistance to PIs, sensitivity to PARP inhibitors, NOTCH proteins, HECT E3 ubiquitin ligases, PI3K/AKT/MTOR signaling. In the lower panel statistical significance of mutation prevalence for each gene group are indicated. Details on composition of gene groups are given in supplemental Table S4.

**Suppl. Figure S4. Mutations in gene group 'IMiD resistance' in RRMM.**

Genes affected by SNVs or Indels in the gene group 'IMiD resistance' and their prevalence in the RRMM cohort are shown as well as copy number aberrations (CNAs) of chromosome arms 13q, 1q, 17p, 1p, presence or absence of hyperdiploid karyotype, and the genomic instability score.

**Suppl. Figure S5. Mutations in gene group 'PI resistance' in RRMM.**

Genes affected by SNVs or Indels in the gene group 'PI resistance' and their prevalence in the RRMM cohort are shown as well as copy number aberrations (CNAs) of chromosome arms 13q, 1q, 17p, 1p, presence or absence of hyperdiploid karyotype, and the genomic instability score.

**Suppl. Figure S6. Mutations in gene group 'PARP inhibitor sensitivity' in RRMM.**

Genes affected by SNVs or Indels in the gene group 'PAPR inhibitor sensitivity' and their prevalence in the RRMM cohort are shown as well as copy number aberrations (CNAs) of chromosome arms 13q, 1q, 17p, 1p, presence or absence of hyperdiploid karyotype, and the genomic instability score.

**Suppl. Figure S7. Exposure to mutational signatures in RRMM original data vs RRMM subsampled data vs NDMM.**

A. The absolute exposure to mutational signatures based on the Alexandrov COSMIC (AC) catalogue with the addition of the MM1 signature recently linked to melphalan exposure is shown for RRMM, both original data (orange) and subsampled dataset (blue), vs RMM (green) vs NDMM (red) patients. Most notable is an increased impact of signatures AC3 (light brown) and MM1 (black) in RRMM.
B. HRDetect scores in RRMM, both original data (orange) and subsampled dataset (blue), vs RMM (green) vs NDMM (red) patients.

**Suppl. Figure S8. Highly complex IGL translocation in patient RRMM_34.**

Translocations involving the immunoglobulin heavy chain (IGH) locus and the lambda light chain (IGL) are shown. Orange lines represent immunoglobulin locus translocations, purple lines represent secondary immunoglobulin locus related translocations, and names of partner genes are given. Secondary translocations of the immunoglobulin loci were defined as secondary events with one of the breakpoints of the SV not further away than 2MB from the target breakpoint of a given primary immunoglobulin translocation (i.e. IG —PrimarySV—> PrimaryTarget —SecondarySV—

>SecondaryTarget). To allow for better readability, relative size of chromosomes 11, 12, 14, and 22 are increased.

**Suppl. Figure S9. *FAM46C* rearrangements in RRMM and expression analysis of target genes.**

A. *FAM46C* rearrangements in RRMM. Green lines represent translocations, blue lines deletions, red lines duplications, and black lines inversions. Names of partner genes of interest are given, notable are *FAM46C*;*MYC* translocations. To allow for better readability, relative size of chromosome 1 is increased.
B. Gene expression profile of the *LMO4* gene across the RRMM cohort. The case with the putative enhancer hijacking of the *FAM46C* enhancer shows a markedly increased LMO4 expression.

**Suppl. Figure S10. Gene expression of *MYC* (A), *CD40* (B), *H2AFJ* (C), *CXCR4* (D), *KMT2A* (E), and *CREBL2* (F) as opposed to expression of *MYCN*.**

Expression of *MYC, CD40, H2AFJ*, *CXCR4, KMT2A,* and *CREBL2* for individual RRMM patients is shown by red lines, expression of *MYCN* by blue lines.

## *Supplementary Tables*

**Suppl. Table S1. Patient characteristics of RRMM cohort.**

**Suppl. Table S2. Detailed information on small variants in RRMM cohort as Excel file.**

Legend for table columns is as follows:

| | |
|---|---|
| PID | |
| VAR_TYPE | SNVs or Indels |
| CHROM | |
| POS | |
| REF | |
| ALT | |
| VAR_SOURCE | Source of the somatic variant: Either from default somatic workflow or from TiNDA rescue |
| ANNOVAR_FUNCTION | Exonic or splicing |
| GENE | Gene name |
| EXONIC_CLASSIFICATION | Exonic protein sequence altering type |
| ANNOVAR_TRANSCRIPTS | Transcript information |
| Tumor_VAF | Tumor variant allele frequency (VAF) |
| Control_VAF | Control VAF |
| RNA_VAF | VAF in RNAseq data |
| ANNOTATION_RNA | Annotation tag about the expression status of the variant |
| CADD_PHRED | CADD (v1.3) score in Phred scale |
| gnomAD_MAF | GnomAD (v2.1) genome MAF |
| HYPER_DIPLOID | Hyper diploid sample classification |
| GENOMIC_INSTABILITY_SCORE | Genomic instability sample score |
| HRDetect | Genomic instability sample-level scores from HRDetect workflow |
| abs_AC3 | Absolute AC3 mutational signature for the sample |
| norm_AC3 | Normalized AC3 mutational signature for the sample |

VAF: Variant allele frequency; MAF: Minor allele frequency; HRD: Homologous recombination deficiency; LST: Large-scale transition; TAI: Telomeric allelic imbalance; AC3: Alexandrov COSMIC signature 3

**Suppl. Table S3. Analysis of mono- vs bi-allelic events.**

**Suppl. Table S4. Composition of gene groups and networks.**

**Suppl. Table S5. Detailed information on small variants in gene groups 'IMiD resistance', 'PI resistance', and 'PARP inhibitor sensitivity' in RRMM cohort as Excel file.**

Legend for table columns as described for suppl. Table S2.

**Suppl. Table S6. Mutational signatures and asserted mutational mechanisms in RRMM cohort.**

**suppl. Figure S1**

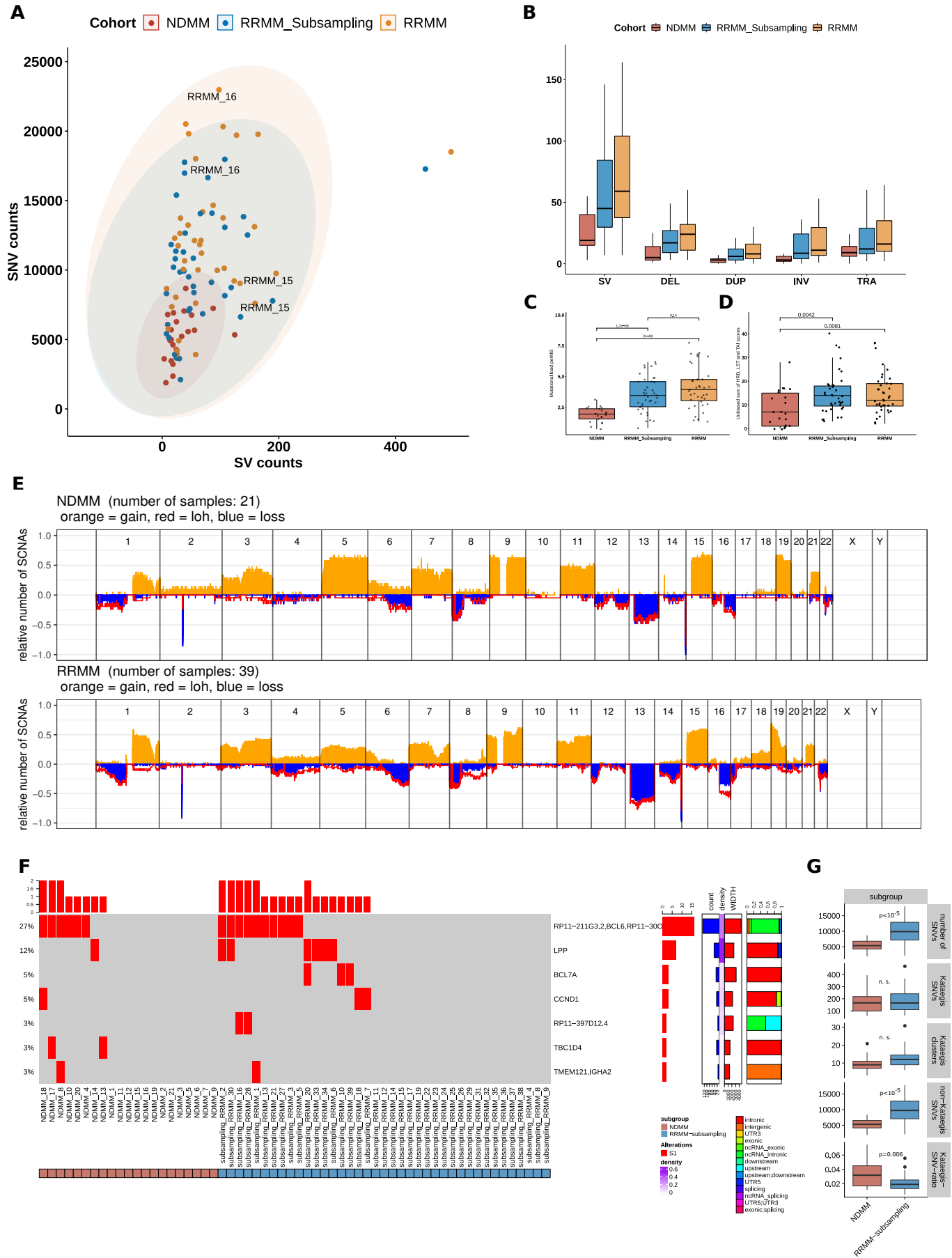

**suppl. Figure S2**

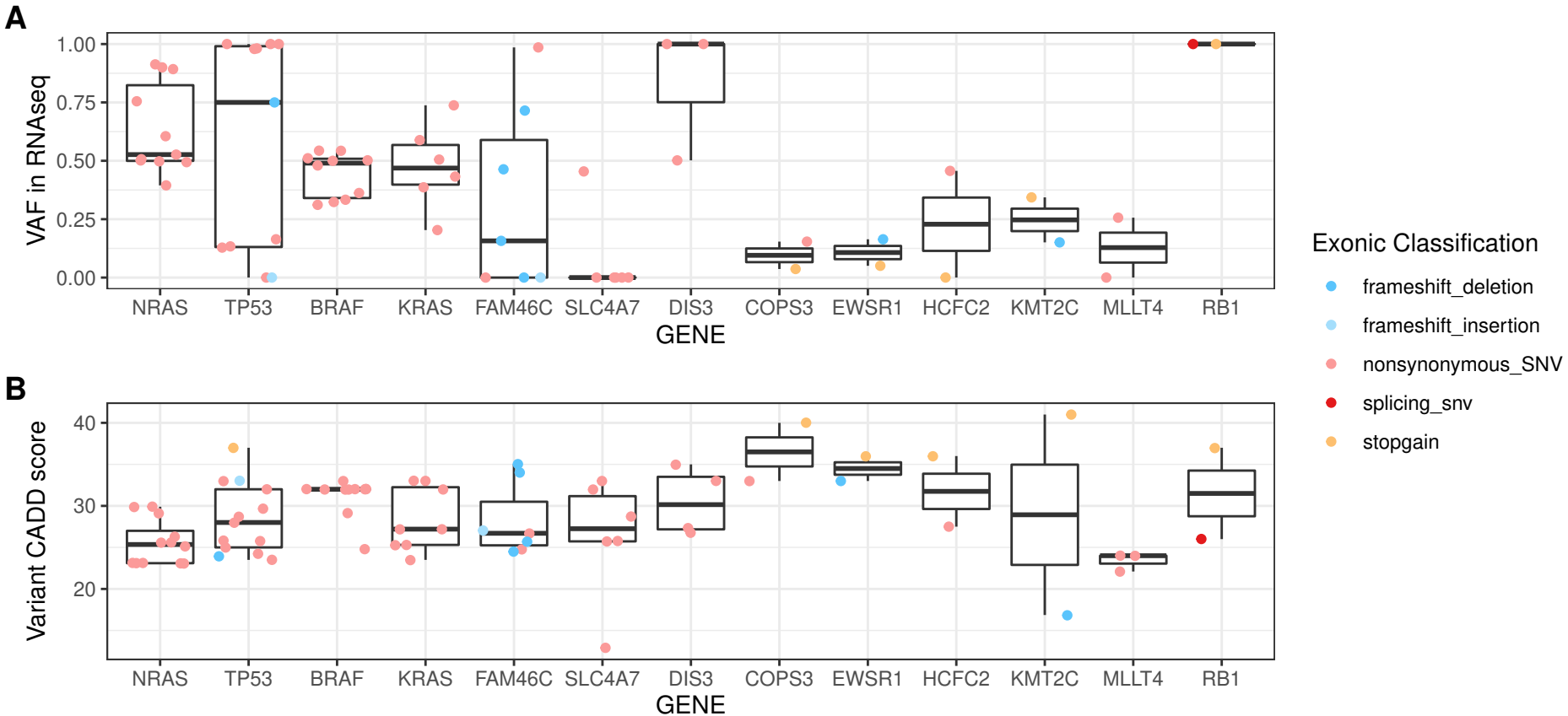

**suppl. Figure S3**

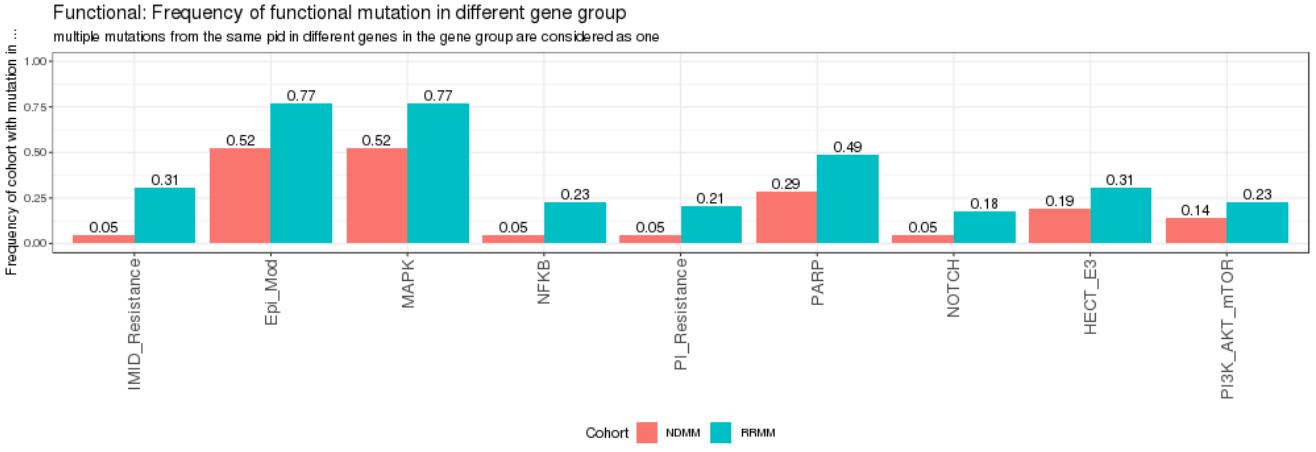


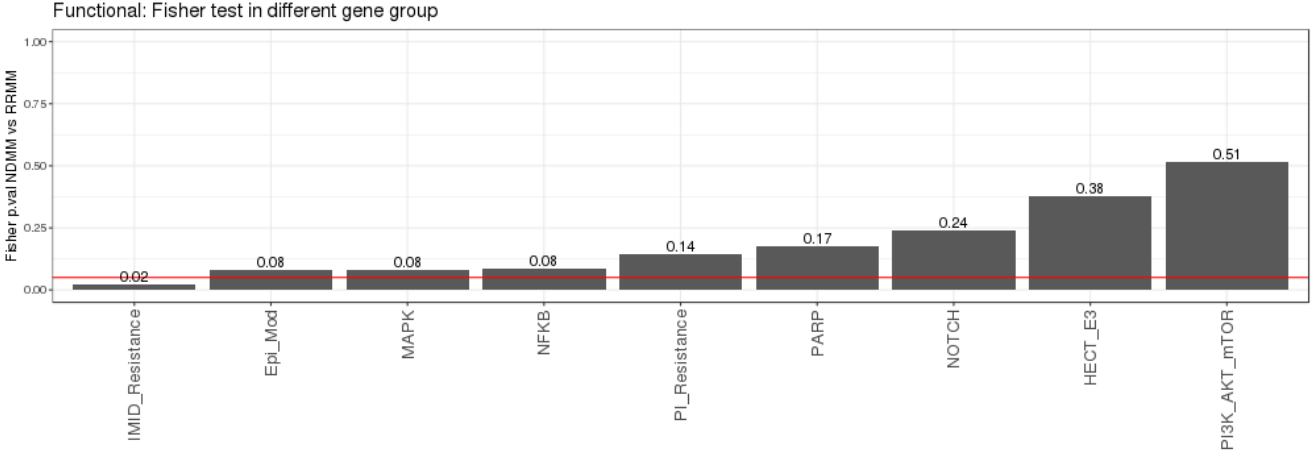

**suppl. Figure S4**

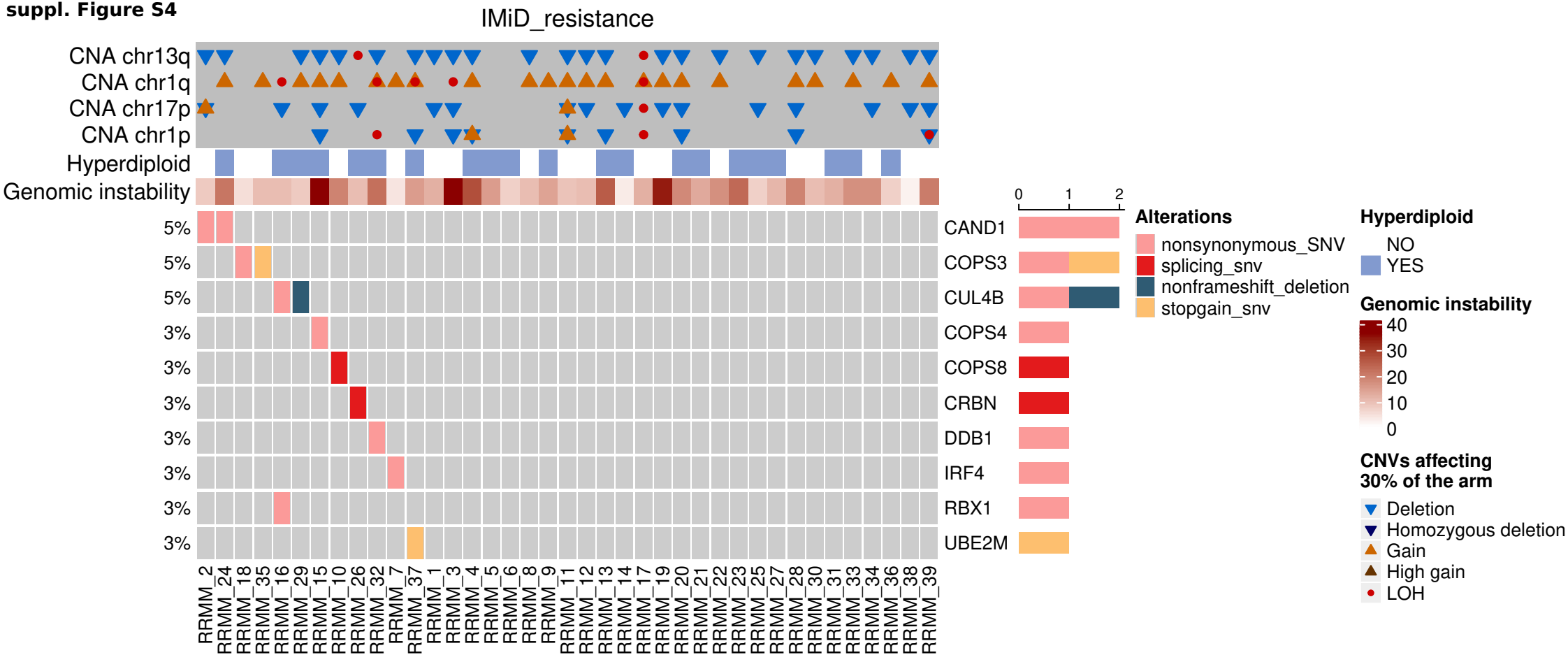

**suppl. Figure S5**

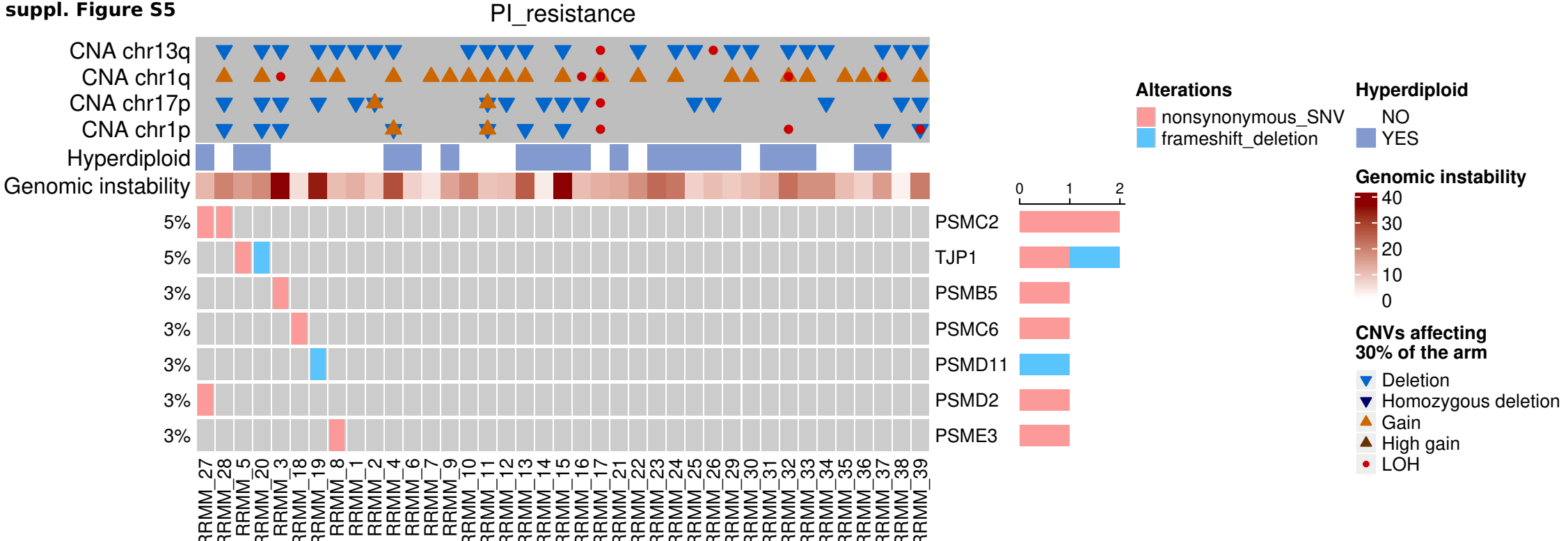

**suppl. Figure S6**

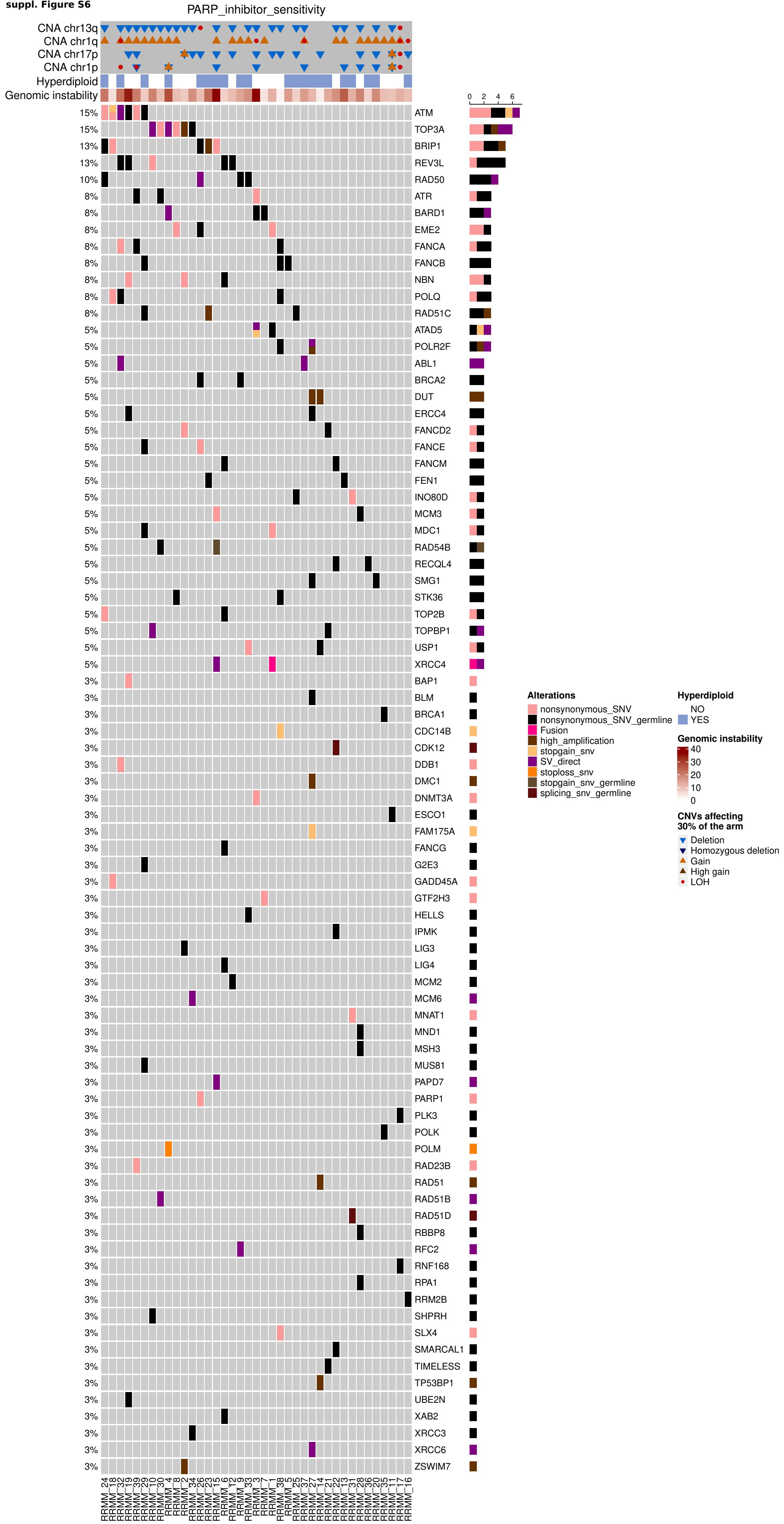

**suppl. Figure S7**

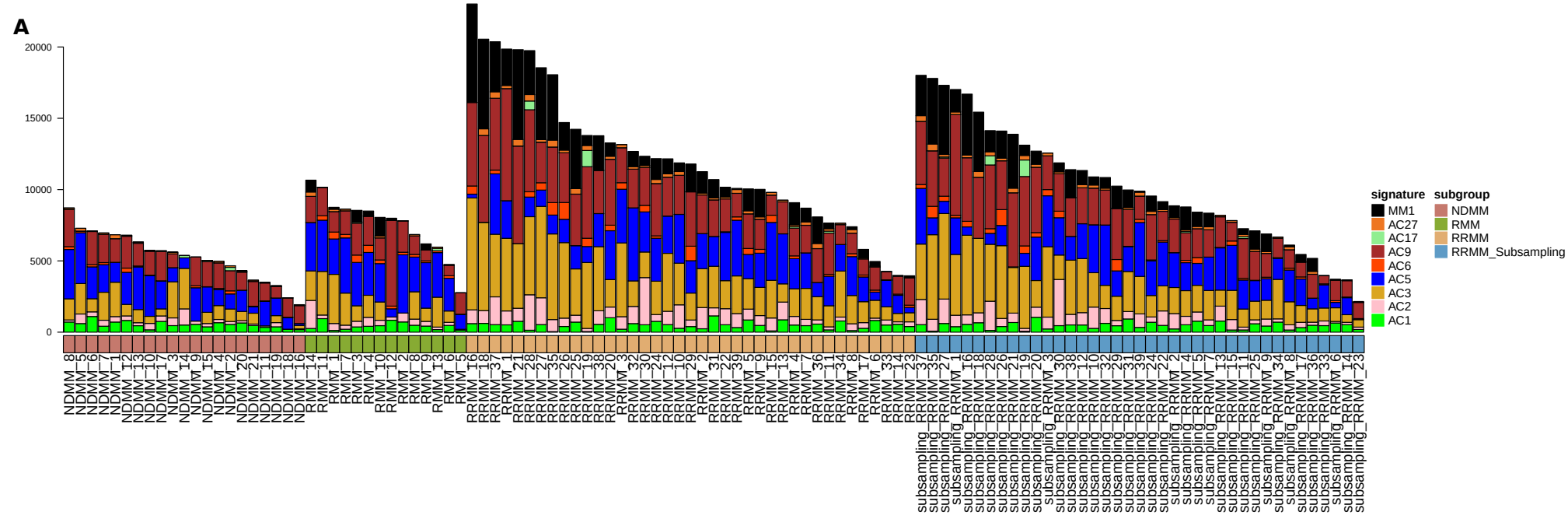


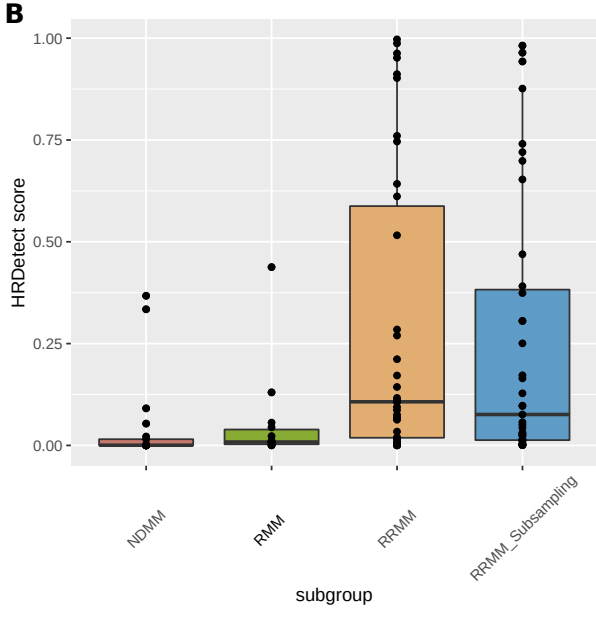

**suppl. Figure S8**

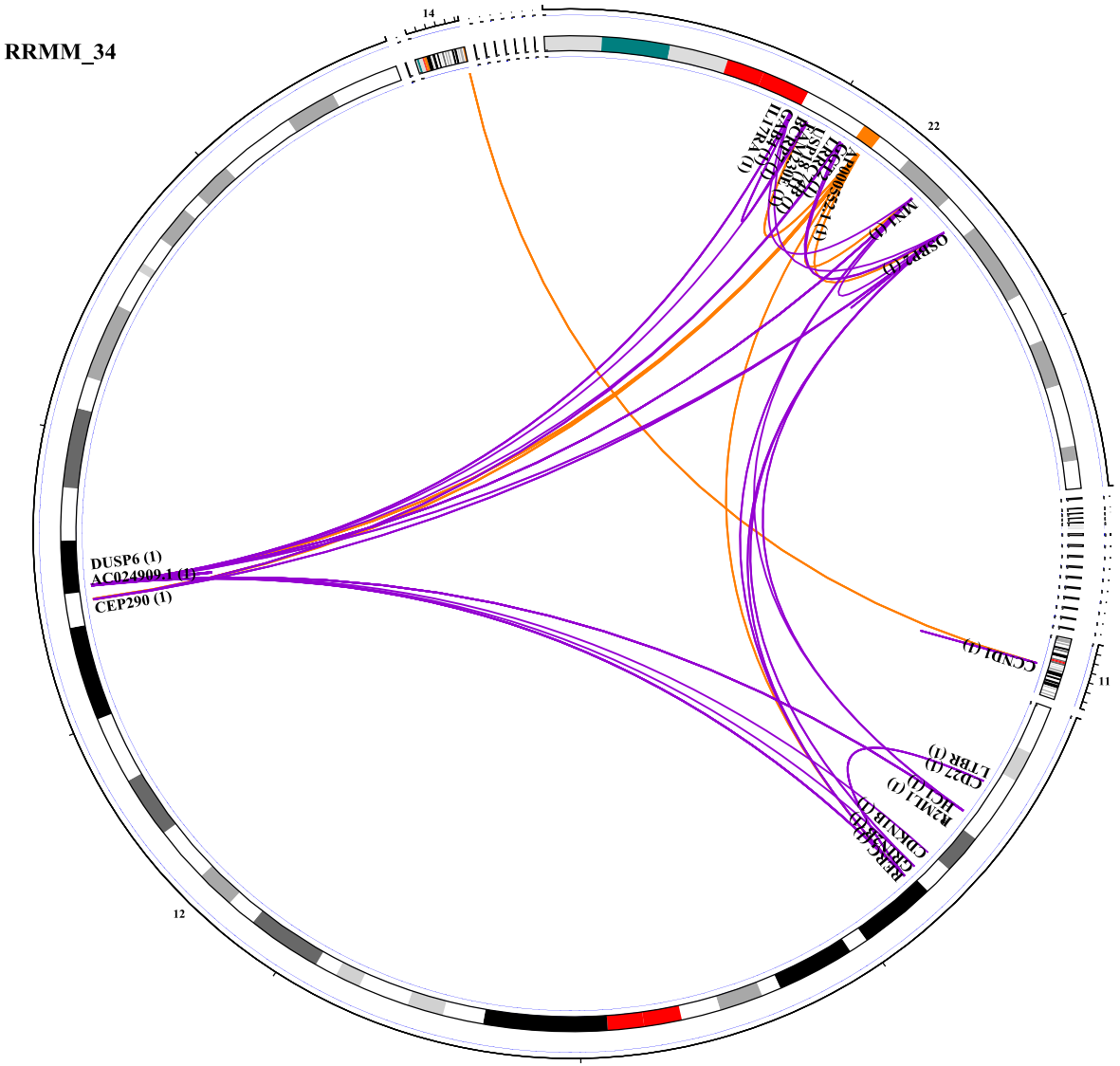

**suppl. Figure S9**

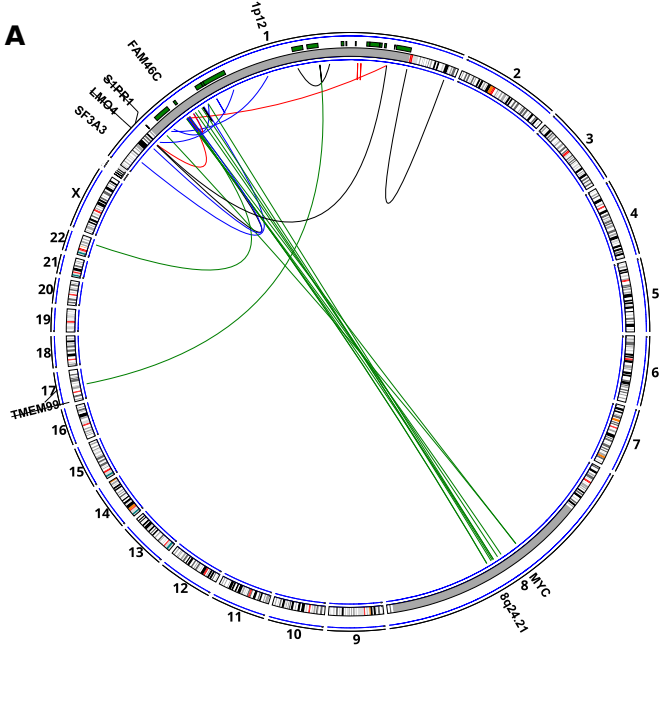


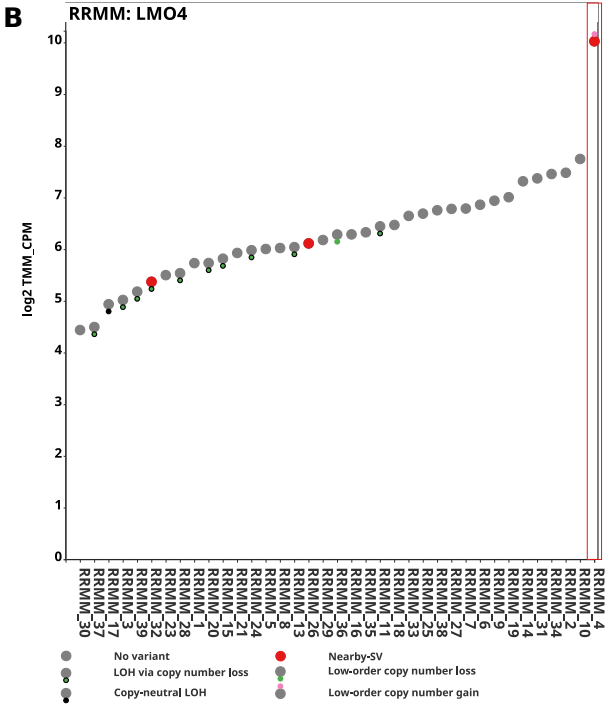

# suppl. Figure S10

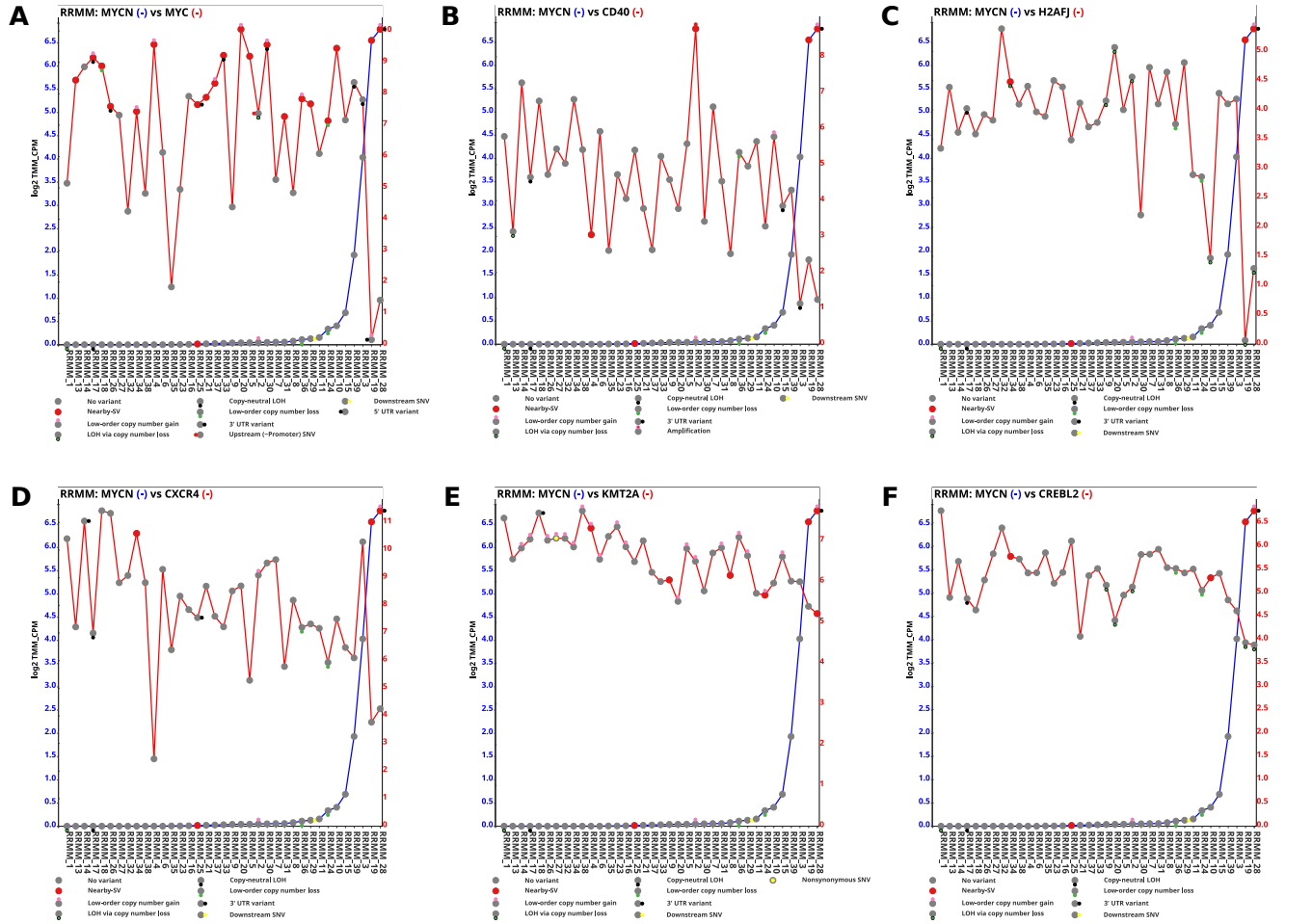

**Suppl. Table S1: Patient characteristics of RRMM cohort.**

| ID | age (years) | sex | time from diagnosis (years) | MM type | ISS | hyperdiploid karyotype | high-risk cytogenetics at RRMM by FISH | #prior therapies | last therapy | prior IMID | prior PI | prior ASCT | refr to LEN | refr to POM | refr to BTZ | refr to CFZ | refr to CD38 | part of cohort of Kortuem *et al.* (1) |
|---|---|---|---|---|---|---|---|---|---|---|---|---|---|---|---|---|---|---|
| RRMM_1 | 68 | male | 3,2 | BJ lambda | 2 | no | del(17p) | 6 | CFZ-Dex | yes | yes | yes | yes | yes | yes | yes | no | no |
| RRMM_2 | 74 | male | 5,5 | IgA kappa | 2 | no | del(17p), t(4;14) | 4 | CFZ-Dex | yes | yes | yes | yes | no | yes | yes | no | yes |
| RRMM_3 | 40 | male | 1,5 | IgG kappa | 2 | no | del(17p) | 2 | LEN-Cy-Dex | yes | yes | yes | yes | no | yes | no | no | no |
| RRMM_4 | 65 | female | 3,2 | IgG kappa | 3 | yes | no | 5 | CFZ-Dex | yes | yes | yes | yes | yes | yes | yes | no | no |
| RRMM_5 | 70 | female | 6,2 | IgG lambda | 2 | yes | no | 4 | POM-Cy-Dex | yes | yes | yes | yes | yes | no | yes | no | no |
| RRMM_6 | 56 | male | 10,1 | IgG kappa | 1 | yes | no | 4 | POM-Dex | yes | yes | yes | yes | yes | no | no | no | no |
| RRMM_7 | 59 | male | 7,3 | IgG kappa | 1 | no | no | 5 | CFZ-LEN-Dex | yes | yes | yes | yes | no | yes | yes | no | no |
| RRMM_8 | 78 | male | 4,7 | BJ lambda | 3 | no | >3 copies 1q21 | 6 | CFZ-Dex | yes | yes | no | yes | yes | yes | yes | no | no |
| RRMM_9 | 67 | male | 16,0 | IgA kappa | na | yes | no | 8 | POM-Dex | yes | yes | yes | yes | yes | yes | yes | no | yes |
| RRMM_10 | 73 | female | 4,1 | IgG kappa | 2 | no | del(17p), >3 copies 1q21, t(4;14) | 8 | CFZ-Dex | yes | yes | yes | yes | yes | yes | yes | no | no |
| RRMM_11 | 71 | male | 3,9 | IgA lambda | 3 | no | >3 copies 1q21, t(4;14) | 5 | POM-Dex | yes | yes | yes | yes | yes | yes | no | no | yes |
| RRMM_12 | 76 | female | 7,4 | IgG kappa | na | no | >3 copies 1q21 | 9 | POM-Dex | yes | yes | no | no | yes | yes | no | no | no |
| RRMM_13 | 78 | female | 2,2 | IgG kappa | 2 | yes | no | 3 | CD38-POM-Dex | yes | yes | no | yes | yes | yes | no | yes | no |
| RRMM_14 | 63 | female | 1,8 | IgA lambda | 2 | yes | del(17p) | 3 | CFZ-Cy-Dex | yes | yes | yes | yes | no | no | yes | no | no |
| RRMM_15 | 49 | male | 1,3 | IgG kappa | 2 | yes | del(17p), >3 copies 1q21 | 4 | POM-Dex | yes | yes | yes | yes | yes | yes | no | no | no |
| RRMM_16 | 75 | male | 11,1 | IgG kappa | na | yes | del(17p) | 8 | CFZ-Dex | yes | yes | yes | yes | yes | yes | yes | no | no |
| RRMM_17 | 55 | female | 1,4 | IgG kappa | 1 | no | del(17p) | 3 | POM-Dex | yes | yes | yes | yes | yes | yes | no | no | no |
| RRMM_18 | 67 | female | 9,5 | IgG lambda | 1 | no | no | 6 | CFZ-LEN-Dex | yes | yes | yes | yes | yes | yes | yes | no | no |
| RRMM_19 | 66 | male | 3,9 | IgA lambda | 3 | no | del(17p), t(4;14) | 4 | SLAMF7-POM-Dex | yes | yes | yes | yes | yes | yes | yes | no | no |
| RRMM_20 | 65 | female | 4,2 | IgG kappa | 1 | yes | del(17p), >3 copies 1q21 | 3 | POM-Dex | yes | yes | yes | no | yes | yes | no | no | yes |
| RRMM_21 | 64 | female | 12,8 | IgG kappa | na | yes | no | 6 | CFZ-LEN-Dex | yes | yes | yes | yes | no | no | yes | no | no |
| RRMM_22 | 69 | male | 4,2 | IgG lambda | 2 | no | del(17p), t(4;14) | 11 | Ruxolitinib | yes | yes | yes | yes | yes | yes | yes | no | no |
| RRMM_23 | 77 | male | 12,9 | IgA lambda | 3 | yes | no | 7 | POM-Dex | yes | yes | yes | yes | yes | no | no | no | no |
| RRMM_24 | 68 | male | 5,9 | IgG kappa | 3 | yes | >3 copies 1q21 | 5 | POM-Dex | yes | yes | yes | yes | yes | yes | no | no | no |
| RRMM_25 | 53 | female | 8,6 | IgG kappa | 2 | yes | del(17p) | 8 | POM-Dex | yes | yes | yes | yes | yes | yes | yes | no | yes |
| RRMM_26 | 54 | male | 2,1 | IgG kappa | 3 | yes | no | 3 | POM-Dex | yes | yes | yes | yes | yes | no | no | no | yes |
| RRMM_27 | 62 | female | 4,4 | IgG kappa | 1 | yes | no | 4 | POM-Dex | yes | yes | yes | no | yes | yes | no | no | no |
| RRMM_28 | 47 | male | 1,9 | BJ lambda | na | no | del(17p), >3 copies 1q21, t(4;14) | 3 | CFZ-LEN-Dex | yes | yes | yes | yes | no | yes | yes | no | no |
| RRMM_29 | 67 | female | 6,8 | IgG kappa | na | yes | no | 9 | CFZ-Dex | yes | yes | yes | yes | yes | yes | yes | no | no |
| RRMM_30 | 51 | male | 4,4 | BJ lambda | na | no | >3 copies 1q21 | 8 | CFZ-Dex | yes | yes | yes | yes | yes | no | yes | no | no |
| RRMM_31 | 53 | male | 6,8 | IgG kappa | 2 | yes | no | 5 | CFZ-Dex | yes | yes | yes | yes | no | no | yes | no | yes |
| RRMM_32 | 85 | female | 13,2 | BJ lambda | 1 | yes | no | 13 | CFZ-Cy-Dex | yes | yes | no | yes | yes | yes | yes | no | yes |
| RRMM_33 | 48 | female | 1,7 | IgG lambda | na | yes | no | 5 | CFZ-Dex | yes | yes | yes | yes | yes | yes | yes | no | yes |
| RRMM_34 | 63 | female | 3,4 | IgG lambda | 1 | no | del(17p) | 3 | POM-Dex | yes | yes | yes | yes | yes | yes | yes | no | no |
| RRMM_35 | 42 | female | 7,0 | IgG lambda | 1 | no | no | 13 | CD38-LEN-Dex | yes | yes | yes | yes | yes | yes | yes | yes | no |
| RRMM_36 | 38 | male | 2,4 | IgA lambda | 3 | yes | no | 5 | BTZ-THA-Dex-PACE | yes | yes | yes | yes | no | yes | yes | no | no |
| RRMM_37 | 70 | male | 5,0 | IgA kappa | 1 | yes | no | 5 | CFZ-Dex | yes | yes | yes | yes | no | no | yes | no | no |
| RRMM_38 | 60 | male | 9,6 | IgG kappa | 1 | no | del(17p) | 4 | LEN-Dex | yes | yes | yes | yes | no | yes | no | no | no |
| RRMM_39 | 64 | female | 3,3 | BJ kappa | 1 | no | del(17p) | 5 | POM-Dex | yes | yes | no | yes | yes | yes | no | yes | no |

abbreviations: MM - multiple myeloma; BJ - bence jones; ISS - international staging system; na - not available; CFZ - carfilzomib; Dex - dexamethasone; LEN - lenalidomide; Cy - cyclophosphamide; POM - pomalidomide; CD38 - anti-CD38 monoclonal antibody; SLAMF7 - anti-SLAMF7 monoclonal antibody; BTZ - bortezomib; THA - thalidomide; PACE - cisplatin, adriamycin, cyclophosphamide, etoposide; IMID - immunomodulatory agent; PI - proteasome inhibitor; ASCT - autologous stem cell transplantation; refr - refractory. (1) Kortüm et al. Blood 2016, Targeted sequencing of refractory myeloma reveals a high incidence of mutations in CRBN and Ras pathway genes.

**Suppl. Table S3: Analysis of mono- vs bi-allelic events.**

| ID | CDKN2C | FAM46C | ASXL2 | BIRC2 | RB1 | PCDH17 | TRAF3 | CYLD | WWOX | TP53 | NF1 | IGLL5 | SNX29 | NBAS | MMRN1 |
|---|---|---|---|---|---|---|---|---|---|---|---|---|---|---|---|
| RRMM_1 | wildtype | wildtype | bi-allelic | wildtype | mono-allelic | mono-allelic | wildtype | wildtype | wildtype | mono-allelic | mono-allelic | mono-allelic | wildtype | bi-allelic | wildtype |
| RRMM_2 | wildtype | wildtype | wildtype | wildtype | mono-allelic | mono-allelic | mono-allelic | mono-allelic | mono-allelic | bi-allelic | wildtype | wildtype | wildtype | wildtype | wildtype |
| RRMM_3 | mono-allelic | mono-allelic | wildtype | wildtype | mono-allelic | mono-allelic | bi-allelic | wildtype | wildtype | bi-allelic | bi-allelic | mono-allelic | wildtype | wildtype | mono-allelic |
| RRMM_4 | wildtype | mono-allelic | wildtype | wildtype | bi-allelic | mono-allelic | wildtype | mono-allelic | mono-allelic | wildtype | wildtype | wildtype | wildtype | wildtype | bi-allelic |
| RRMM_5 | wildtype | bi-allelic | wildtype | wildtype | wildtype | wildtype | wildtype | mono-allelic | mono-allelic | wildtype | wildtype | mono-allelic | wildtype | wildtype | wildtype |
| RRMM_6 | wildtype | mono-allelic | wildtype | wildtype | wildtype | wildtype | wildtype | wildtype | wildtype | wildtype | wildtype | wildtype | wildtype | wildtype | mono-allelic |
| RRMM_7 | wildtype | wildtype | wildtype | wildtype | mono-allelic | mono-allelic | wildtype | wildtype | wildtype | wildtype | wildtype | wildtype | wildtype | wildtype | wildtype |
| RRMM_8 | wildtype | wildtype | wildtype | bi-allelic | mono-allelic | mono-allelic | wildtype | wildtype | wildtype | wildtype | wildtype | mono-allelic | wildtype | wildtype | wildtype |
| RRMM_9 | wildtype | wildtype | wildtype | mono-allelic | wildtype | wildtype | wildtype | wildtype | wildtype | wildtype | wildtype | mono-allelic | wildtype | wildtype | wildtype |
| RRMM_10 | wildtype | mono-allelic | wildtype | wildtype | bi-allelic | bi-allelic | wildtype | mono-allelic | wildtype | bi-allelic | wildtype | mono-allelic | wildtype | wildtype | wildtype |
| RRMM_11 | mono-allelic | mono-allelic | wildtype | wildtype | mono-allelic | mono-allelic | bi-allelic | wildtype | wildtype | mono-allelic | wildtype | bi-allelic | wildtype | wildtype | wildtype |
| RRMM_12 | wildtype | wildtype | wildtype | mono-allelic | bi-allelic | mono-allelic | wildtype | wildtype | wildtype | mono-allelic | wildtype | wildtype | wildtype | wildtype | wildtype |
| RRMM_13 | wildtype | mono-allelic | wildtype | wildtype | mono-allelic | bi-allelic | wildtype | wildtype | wildtype | wildtype | mono-allelic | bi-allelic | wildtype | wildtype | wildtype |
| RRMM_14 | wildtype | wildtype | wildtype | wildtype | bi-allelic | wildtype | wildtype | mono-allelic | mono-allelic | bi-allelic | wildtype | bi-allelic | wildtype | wildtype | wildtype |
| RRMM_15 | bi-allelic | mono-allelic | wildtype | wildtype | mono-allelic | mono-allelic | wildtype | mono-allelic | mono-allelic | bi-allelic | wildtype | wildtype | bi-allelic | wildtype | mono-allelic |
| RRMM_16 | wildtype | wildtype | wildtype | wildtype | wildtype | wildtype | wildtype | wildtype | wildtype | mono-allelic | mono-allelic | wildtype | wildtype | wildtype | wildtype |
| RRMM_17 | wildtype | wildtype | wildtype | wildtype | wildtype | wildtype | wildtype | wildtype | wildtype | bi-allelic | wildtype | bi-allelic | wildtype | wildtype | wildtype |
| RRMM_18 | wildtype | wildtype | wildtype | wildtype | wildtype | wildtype | wildtype | bi-allelic | mono-allelic | wildtype | wildtype | mono-allelic | wildtype | wildtype | wildtype |
| RRMM_19 | wildtype | mono-allelic | mono-allelic | wildtype | mono-allelic | mono-allelic | mono-allelic | mono-allelic | mono-allelic | bi-allelic | wildtype | bi-allelic | wildtype | bi-allelic | wildtype |
| RRMM_20 | mono-allelic | mono-allelic | wildtype | wildtype | mono-allelic | mono-allelic | wildtype | wildtype | wildtype | mono-allelic | wildtype | mono-allelic | wildtype | wildtype | wildtype |
| RRMM_21 | wildtype | wildtype | wildtype | wildtype | wildtype | wildtype | wildtype | wildtype | wildtype | mono-allelic | wildtype | mono-allelic | mono-allelic | wildtype | wildtype |
| RRMM_22 | wildtype | wildtype | wildtype | wildtype | mono-allelic | mono-allelic | wildtype | wildtype | wildtype | wildtype | wildtype | bi-allelic | wildtype | wildtype | wildtype |
| RRMM_23 | wildtype | mono-allelic | wildtype | wildtype | mono-allelic | wildtype | wildtype | wildtype | wildtype | wildtype | wildtype | wildtype | wildtype | wildtype | wildtype |
| RRMM_24 | wildtype | mono-allelic | wildtype | wildtype | mono-allelic | mono-allelic | wildtype | mono-allelic | mono-allelic | wildtype | wildtype | wildtype | wildtype | wildtype | mono-allelic |
| RRMM_25 | wildtype | wildtype | wildtype | wildtype | bi-allelic | mono-allelic | wildtype | mono-allelic | mono-allelic | mono-allelic | wildtype | wildtype | wildtype | wildtype | mono-allelic |
| RRMM_26 | wildtype | wildtype | wildtype | wildtype | wildtype | wildtype | wildtype | bi-allelic | wildtype | mono-allelic | wildtype | wildtype | wildtype | wildtype | wildtype |
| RRMM_27 | wildtype | wildtype | wildtype | wildtype | wildtype | wildtype | wildtype | wildtype | wildtype | wildtype | wildtype | bi-allelic | wildtype | wildtype | wildtype |
| RRMM_28 | wildtype | mono-allelic | wildtype | wildtype | bi-allelic | mono-allelic | wildtype | wildtype | wildtype | mono-allelic | wildtype | bi-allelic | wildtype | mono-allelic | wildtype |
| RRMM_29 | wildtype | mono-allelic | wildtype | wildtype | mono-allelic | mono-allelic | wildtype | wildtype | wildtype | wildtype | wildtype | wildtype | wildtype | wildtype | wildtype |
| RRMM_30 | wildtype | bi-allelic | wildtype | wildtype | mono-allelic | mono-allelic | bi-allelic | wildtype | mono-allelic | wildtype | wildtype | bi-allelic | wildtype | wildtype | wildtype |
| RRMM_31 | wildtype | wildtype | wildtype | wildtype | wildtype | wildtype | wildtype | wildtype | wildtype | wildtype | wildtype | wildtype | wildtype | wildtype | wildtype |
| RRMM_32 | wildtype | wildtype | wildtype | wildtype | mono-allelic | mono-allelic | wildtype | bi-allelic | mono-allelic | wildtype | wildtype | bi-allelic | wildtype | wildtype | wildtype |
| RRMM_33 | wildtype | mono-allelic | wildtype | wildtype | mono-allelic | mono-allelic | bi-allelic | wildtype | wildtype | wildtype | wildtype | bi-allelic | wildtype | wildtype | wildtype |
| RRMM_34 | wildtype | wildtype | wildtype | wildtype | mono-allelic | mono-allelic | wildtype | wildtype | mono-allelic | bi-allelic | mono-allelic | wildtype | wildtype | wildtype | wildtype |
| RRMM_35 | wildtype | wildtype | wildtype | wildtype | wildtype | wildtype | wildtype | bi-allelic | wildtype | wildtype | wildtype | bi-allelic | wildtype | wildtype | wildtype |
| RRMM_36 | wildtype | wildtype | wildtype | wildtype | wildtype | wildtype | wildtype | mono-allelic | mono-allelic | wildtype | wildtype | bi-allelic | wildtype | wildtype | wildtype |
| RRMM_37 | mono-allelic | mono-allelic | wildtype | wildtype | bi-allelic | mono-allelic | bi-allelic | mono-allelic | mono-allelic | wildtype | wildtype | wildtype | wildtype | wildtype | wildtype |
| RRMM_38 | wildtype | wildtype | wildtype | wildtype | mono-allelic | bi-allelic | wildtype | wildtype | wildtype | mono-allelic | wildtype | wildtype | wildtype | wildtype | wildtype |
| RRMM_39 | mono-allelic | mono-allelic | wildtype | wildtype | mono-allelic | mono-allelic | bi-allelic | wildtype | wildtype | mono-allelic | wildtype | wildtype | wildtype | wildtype | wildtype |

**Suppl. Table S4: Composition of gene groups and networks.**

| resistance to PIs | resistance to IMiDs | PARP inhibitor sensitivity | | | | MAPK pathway | NFKB signaling |
|---|---|---|---|---|---|---|---|
| PSMC1 | CRBN | ABL1 | GEN1 | PRMT6 | USP7 | ARAF | REL |
| PSMC2 | IZKF1 | ATAD5 | GIYD1 | PSMC3IP | WRN | BRAF | RELA |
| PSMC3 | IZKF3 | ATM | GIYD2 | PTEN | XAB2 | RAF1 | RELB |
| PSMC4 | IRF4 | ATR | GTF2H3 | RAD21 | XRCC2 | MAP2K1 | NFKB1 |
| PSMC5 | CUL4A | AURORA | HELLS | RAD23B | XRCC3 | MAP2K2 | NFKB2 |
| PSMC6 | CUL4B | BAP1 | HUS1 | RAD50 | XRCC4 | MAPK1 | IKBKB |
| TJP1 | DDB1 | BARD1 | INIP | RAD51 | XRCC6 | MAPK3 | CHUK |
| PSMB9 | RBX1 | BLM | INO80D | RAD51B | ZSWIM7 | HRAS | IKBKG |
| PSMB8 | COPS1 | BRCA1 | IPMK | RAD51C | | KRAS | NFKBIA |
| PSMB5 | COPS2 | BRCA2 | KAT5 | RAD51D | | NRAS | TRADD |
| ERN1 | COPS3 | BRCC3 | LIG3 | RAD52 | | SOS1 | RIPK1 |
| XBP1 | COPS4 | BRIP1 | LIG4 | RAD54B | | SOS2 | TRAF2 |
| PSMA1 | COPS5 | CDC14B | MAD2L2 | RAD54L | | NF1 | TRAF5 |
| PSMA2 | COPS6 | CDK12 | MAPK12 | RBBP8 | | GRB2 | MAP3K14 |
| PSMA3 | COPS7 | CDK5 | MCM2 | RECQL4 | | RASA1 | BIRC2 |
| PSMA4 | COPS8 | CDK7 | MCM3 | REV3L | | RASA2 | BIRC3 |
| PSMA5 | CAND1 | CHEK1 | MCM6 | RFC2 | | PTPN11 | TRAF3 |
| PSMA6 | UBE2M | CHEK2 | MDC1 | RNF168 | | RASGRF1 | TRAF1 |
| PSMA7 | UBE2D3 | DDB1 | miR-103 | RPA1 | | RASGRF2 | TRAF6 |
| PSMA8 | UBE2G1 | DMC1 | miR-107 | RRM1 | | RASGRP1 | TAK1 |
| PSMB1 | | DNASE1L2 | miR-222 | RRM2B | | RASGRP2 | NFKBIB |
| PSMB2 | | DNMT3A | miR-506 | SHFM1 | | RASGRP3 | NFKBIE |
| PSMB3 | | DUT | miR-9 | SHPRH | | RASGRP4 | IRAK1 |
| PSMB4 | | EME1 | MMS22L | SLX4 | | RASAL1 | TRAF7 |
| PSMB6 | | EME2 | MNAT1 | SMARCA2 | | RASAL2 | RIPK2 |
| PSMB7 | | ERCC1 | MND1 | SMARCA5 | | RASA4 | RIPK3 |
| PSMB10 | | ERCC4 | MRE11A | SMARCAL1 | | RASA3 | |
| PSMB11 | | ERCC8 | MSH3 | SMC3 | | | |
| PSMD1 | | ESCO1 | MUM1 | SMG1 | | | |
| PSMD2 | | ESCO2 | MUS81 | SPO11 | | | |
| PSMD3 | | EWSR1-FLI1 | NAMPT | SSRP1 | | | |
| PSMD4 | | FAAP20 | NAP1L1 | STK36 | | | |
| PSMD7 | | FAAP24 | NBN | SUMO1 | | | |
| PSMD8 | | FAM175A | ORC1L | TEX11 | | | |
| PSMD11 | | FANCA | ORC5L | TIMELESS | | | |
| PSMD12 | | FANCB | PALB2 | TMPRSS2-ERG | | | |
| PSMD13 | | FANCC | PAPD7 | TOP2B | | | |
| PSMD14 | | FANCD2 | PARP1 | TOP3A | | | |
| PSME1 | | FANCE | PLK3 | TOPBP1 | | | |
| PSME2 | | FANCF | PNKP | TP53BP1 | | | |
| PSME3 | | FANCG | POLB | TTDN1 | | | |
| PSME4 | | FANCI | POLD3 | UBA1 | | | |
| PSMF1 | | FANCL | POLH | UBE2A | | | |
| SHFM1 | | FANCM | POLK | UBE2N | | | |
| ADRM1 | | FEN1 | POLM | UNG | | | |
| | | G2E3 | POLQ | USP1 | | | |
| | | GADD45A | POLR2F | USP10 | | | |

| epigenetic modifiers | | | | | | | |
|---|---|---|---|---|---|---|---|
| HIST1H1A | H2BFM | PHF2 | HDAC5 | ARID1B | CTCF | | |
| HIST1H1B | H2BFWT | PHF8 | HDAC6 | ARID2 | MBD1 | | |
| HIST1H1C | HIST1H3A | ASH1L | HDAC7 | ARID3A | MBD2 | | |
| HIST1H1D | HIST1H3B | CARM1 | HDAC8 | ARID3B | MBD3 | | |
| HIST1H1E | HIST1H3C | DOT1L | HDAC9 | ARID3C | MBD4 | | |
| HIST1H1T | HIST1H3D | EED | SIRT1 | ARID4A | MBD5 | | |
| H1FOO | HIST1H3E | EHMT1 | SIRT2 | ARID4B | MBD6 | | |
| H1FNT | HIST1H3F | EHMT2 | SIRT3 | ARID5A | MECP2 | | |
| H1F0 | HIST1H3G | EZH1 | SIRT4 | ARID5B | RAG2 | | |
| H1FX | HIST1H3H | EZH2 | SIRT5 | ASXL1 | TDG | | |
| HIST1H2AA | HIST1H3I | MEN1 | SIRT6 | ATRX | TP53BP1 | | |
| HIST1H2AB | HIST1H3J | NSD1 | SIRT7 | BRD7 | | | |
| HIST1H2AC | HIST2H3D | PRDM2 | ZBTB33 | CHD1 | | | |
| HIST1H2AD | HIST3H3 | PRMT1 | BRPF1 | CHD2 | | | |
| HIST1H2AE | H3F3A | PRMT2 | CLOCK | CHD3 | | | |
| HIST1H2AG | H3F3B | PRMT5 | CREBBP | CHD4 | | | |
| HIST1H2AH | H3F3C | PRMT6 | ELP3 | CHD5 | | | |
| HIST1H2AJ | HIST1H4A | PRMT7 | EP300 | CHD6 | | | |
| HIST1H2AK | HIST1H4B | SETD1A | EP400 | CHD8 | | | |
| HIST1H2AL | HIST1H4C | SETD1B | GNAT1 | CHD9 | | | |
| HIST1H2AM | HIST1H4D | SETD2 | GNAT2 | DPF1 | | | |
| HIST2H2AB | HIST1H4E | SETD3 | GNAT3 | DPF2 | | | |
| HIST2H2AC | HIST1H4F | SETD7 | GTF3C4 | INO80 | | | |
| HIST3H2A | HIST1H4G | SETD8 | HAT1 | KLF1 | | | |
| H2AFB3 | HIST1H4H | SETDB1 | KAT2A | MLF1IP | | | |
| H2AFJ | HIST1H4I | SETDB2 | KAT2B | PBRM1 | | | |
| H2AFV | HIST1H4J | SETMAR | KAT5 | PHF10 | | | |
| H2AFX | HIST1H4K | SMYD1 | KAT6A | RBBP4 | | | |
| H2AFY | HIST1H4L | SMYD2 | KAT6B | SET | | | |
| H2AFY2 | HIST4H4 | SMYD3 | KAT7 | SMARCA1 | | | |
| H2AFZ | KDM1A | SUV39H1 | KAT8 | SMARCA2 | | | |
| HIST1H2BA | KDM1B | SUV39H2 | MORF4L1 | SMARCA4 | | | |
| HIST1H2BB | KDM2A | SUV420H1 | NCOA1 | SMARCA5 | | | |
| HIST1H2BC | KDM2B | SUV420H2 | NCOA2 | SMARCAD1 | | | |
| HIST1H2BD | KDM3A | SUZ12 | NCOA3 | SMARCAL1 | | | |
| HIST1H2BE | KDM3B | WHSC1 | TAF1 | SMARCB1 | | | |
| HIST1H2BF | KDM4A | WHSC1L1 | TAF1L | SMARCC1 | | | |
| HIST1H2BG | KDM4B | KMT2A | TAF3 | SMARCC2 | | | |
| HIST1H2BH | KDM4C | KMT2D | DNMT1 | SMARCD1 | | | |
| HIST1H2BI | KDM4D | KMT2C | DNMT3A | SMARCD2 | | | |
| HIST1H2BJ | KDM5A | KMT2B | DNMT3B | SMARCD3 | | | |
| HIST1H2BK | KDM5B | KMT2E | IDH1 | SMARCE1 | | | |
| HIST1H2BL | KDM5C | BAZ2A | IDH2 | SRCAP | | | |
| HIST1H2BM | KDM5D | HDAC1 | TET1 | BPTF | | | |
| HIST1H2BN | KDM6A | HDAC10 | TET2 | BRD2 | | | |
| HIST1H2BO | KDM6B | HDAC11 | TET3 | BRD4 | | | |
| HIST2H2BE | KDM7A | HDAC2 | ACTL6A | BRD8 | | | |
| HIST2H2BF | KDM8 | HDAC3 | ACTL6B | CBX5 | | | |
| HIST3H2BB | UTY | HDAC4 | ARID1A | CBX7 | | | |

| PI3K/AKT/ MTOR pathway | NOTCH receptors | HECT E3 ligases | references |
|---|---|---|---|
| PIK3CA | NOTCH1 | NEDD4 | Barrio et al. Leukemia 2018, Spectrum and functional validation of PSMB5 mutations in multiple myeloma. |
| PIK3CB | NOTCH2 | NEDD4L | |
| PIK3CD | NOTCH3 | SMURF1 | Cargnello et al. Microbiol Mol Biol Rev. 2011, Activation and Function of the MAPKs and Their Substrates, the MAPK-Activated Protein Kinases. |
| PIK3R1 | NOTCH4 | SMURF2 | |
| PIK3R2 | | ITCH | Hayden et al. Cell 2008, Shared principles in NF-kappaB signaling. |
| PIK3R3 | | WWP1 | Karin et al. Nature 2006, Nuclear factor-kappaB in cancer development and progression. |
| PIK3R5 | | WWP2 | |
| PIK3R6 | | HECW1 | Karnoub et al. Nat Rev Mol Cell Biol. 2008, Ras oncogenes: split personalities. |
| PIK3CG | | HECW2 | |
| PTEN | | HERC1 | Krönke et al. Science 2014, Lenalidomide Causes Selective Degradation of IKZF1 and IKZF3 in Multiple Myeloma Cells |
| AKT1 | | HERC2 | |
| AKT2 | | HERC3 | Laplante et al. Cell 2012, mTOR Signaling in Growth Control and Disease. |
| AKT3 | | HERC4 | Leung-Hagesteijn et al. Cancer Cell 2013, Xbp1s-Negative Tumor B Cells and Pre-Plasmablasts Mediate Therapeutic Proteasome Inhibitor Resistance in Multiple Myeloma |
| PDK1 | | HERC5 | |
| MTOR | | HERC6 | |
| RICTOR | | UBE3A | Lord et al. Nat Rev Cancer 2016, BRCAness revisited. |
| TCL1A | | UBR5 | Nowell et al. Nat Rev Cancer 2017, Notch as a tumour suppressor. |
| TCL1B | | HACE1 | Pawlyn et al. Clin Cancer Res 2016, The Spectrum and Clinical Impact of Epigenetic Modifier Mutations in Myeloma. |
| PHLPP1 | | HUWE1 | |
| PHLPP2 | | HECT2D | Rotin et al. Nat Rev Mol Cell Biol 2009, Physiological functions of the HECT family of ubiquitin ligases. |
| TSC1 | | HECTD4 | |
| TSC2 | | TRIP12 | Shaw et al. Nature 2006, Ras, PI(3)K and mTOR signalling controls tumour cell growth. |
| RHEB | | G2E3 | |
| RPTOR | | HECTD1 | Shi et al. Mol Cancer Ther 2017, CRISPR Genome-Wide Screening Identifies Dependence on the Proteasome Subunit PSMC6 for Bortezomib Sensitivity in Multiple Myeloma. |
| EIF4EBP1 | | UBE3B | |
| EIF4E | | UBE3C | |
| RPS6KB1 | | AREL1 | Sievers et al. Blood 2018, Genome-wide screen identifies cullin-RING ligase machinery required for lenalidomide-dependent CRL4CRBN activity |
| EIF4B | | HECTD3 | |
| RPS6 | | | |
| MLST8 | | | Sun et al. Cell Res. 2011, Non-canonical NF-κB signaling pathway. |
| AKT1S1 | | | Tanaka et al. 2009, Proc Jpn Acad Ser B Phys Biol Sci:The proteasome: overview of structure and functions. |
| DEPTOR | | | |
| TTI1 | | | Thorpe et al. Nat Rev Cancer 2015, PI3K in cancer: divergent roles of isoforms, modes of activation and therapeutic targeting. |
| TELO2 | | | |
| MAPKAP1 | | | Vigil et al. Nat Rev Cancer 2010, Ras superfamily GEFs and GAPs: validated and tractable targets for cancer therapy? |
| PRR5 | | | |
| PRR5L | | | Zhang et al. Cancer Cell 2016, Tight Junction Protein 1 Modulates Proteasome Capacity and Proteasome Inhibitor Sensitivity in Multiple Myeloma via EGFR/JAK1/STAT3 Signaling. |
| | | | |
| | | | |

**Suppl. Table S6. Mutational signatures and asserted mutational mechanisms in RRMM cohort.**

| Name | Correspondence in COSMIC v2 | colour | Mutational mechanism |
|---|---|---|---|
| AC1 | SBS1 | green | Clock-like; spontaneous deamination |
| AC2 | SBS2 | pink | APOBEC |
| AC3 | SBS3 | gold | Homologous recombination repair deficiency |
| AC5 | SBS5 | blue | Clock-like, mechanism unknown |
| AC6 | SBS6 | orange | Mismatch repair deficiency |
| AC9 | SBS9 | brown | Polymerase η |
| AC17 | SBS17 | lightgreen | mechanism unknown |
| AC27 | SBS27 | chocolate | mechanism unknown |
| MM1 | - | black | melphalan |